BEATING PRIMARY CILIARY DYSKINESIA

BEATRIZ ALEXANDRA ADRIÃO SALVADO

Dissertação para obtenção do grau de Mestre em Bioquímica para a Saúde

setembro, 2022/2023

BEATING PRIMARY CILIARY DYSKINESIA

Beatriz Alexandra Adrião Salvado

Orientadora: Susana Lopes, Investigadora Principal da NOVA Medical School Research

Tese para obtenção do grau de Mestre em Bioquímica para a Saúde

NOVA Medical School Research | Instituto de Medicina Molecular

(Cilia Regulation and Disease Laboratory/NOVA Medical School Research)

setembro, 2022/2023

Acknowledgments

Firstly, I would like to thank my dear supervisor Susana Lopes for welcoming me so well in her laboratory and for her guidance during this work. It was a pleasure working and teaming-up with you over this time. I hope to continue hearing from you and wish that the lab continues to grow! I want to thank Margarida for guiding me through this journey, and having time to always clarify my doubts, even when she was far away. Next, I want to thank Catarina for having all the patience to deal with my doubts and my uncertainties, for listening to me and understanding my insecurities, for always helping me during this journey and for making my lunch times the best! A big thank you to Bárbara, a friend that I made along this tough journey, for being my tea fountain and always making me laugh hard enough to forget the hard times! Last, I want to thank the fish facilities staff that received me so well at Nova Medical School and at IMM. A special thank you to Fábio, Lara and Aida for all the conversations among the fish, for always being ready to help and teach me everything I had to know about the zebrafish world. I really did absorb all the knowledge you had to pass me. I will bring everything that I have learned here for my future both on academic and personal level. Thank you all!

Next, I would like to thank all my friends that have been here for me since day one. For the “university ones”, when we met 5 years ago I wouldn’t imagine that we would still be here all together, stronger and better than ever. Thank you to all my Coolina’s friends! A special thank you to Reta for being my lab partner since day one and for joining me on the same masters to keep the tradition. Thank you Mimosa for always brightening my days at NMS, for the conversations, and specially for the private boutique. Thank you Inês for being the best I could ever ask for, thank you for sharing the good and the bad moments with me! I would also like to thank Renato, Paulo and Kika for being available to listen to me in the middle of the night when necessary. I have the best friends for sure!

I could never forget the support from Joana, Inês and Mariana along all my journey. Thank you for the dinners with endless conversations and for the karaoke we never went to. I stand for what I said 5 years ago: you definitely were my best choice. Thank you too to my 3 beautiful daughters: Rita, I can’t thank you enough for your suport, your kidness and your madness and our endless cringy calls; Cate, our one and only neuron is always going to be our best and stronger feature, thank you

for reminding me how strong I can be; and Catatina thank you for all the singing sessions and for making me believe I can do whatever I want, just like you did, and lastly to my amazing grandson Diogo for always reaching out for me, bringing me the best food and for making me feel special in each conversation. All of you have made my days, for the calls, for the fofocas and for all the food that you bring to surprise me! I couldn't have asked for a better family!

Last, but obviously not least a ginormous thank you to my family, the ones that see me 24/7 as me, that respect my disappearances, my mood swings, my necessities and are always there to give me a hand or the whole body if needed. A special thank you to my big sister, who helped me closely through this journey and kept me motivated to write and to my younger sister with whom I could share everything, even the desk. Thank you to my wonderful parents for making all this possible, for always encouraging me to be and do better. Never settle until I reach my dreams!

Thank you all for making it easier to complete this journey, I could never have done this without any of you! I will keep bothering you all. That is my way of showing how much I care about all of you! Thank you again and again!

Abstract

Primary ciliary dyskinesia (PCD) is a genetic disorder caused by malfunction or absence of motile cilia, which play a key role in the clearance of mucus, bacteria and debris from the respiratory tract. Consequently, individuals with PCD often experience recurrent respiratory infections and bronchiectasis. PCD arises from mutations in a wide array of genes responsible for motile cilia structure and function.

In this work, we tried to identify zebrafish mutants from four PCD genes, namely DNAH 5, DNAH 11, CCDC39 and CCNO, previously created by using a CRISPR-Cas9 approach to mimic human PCD mutations in the homologous site of the zebrafish genome. Since we were not able to find any homozygous mutants from these selected genes during the time-course of my Master project, we focused on F1 *ccdc40*$^{+/-}$ zebrafish mutants already identified to generate homozygous mutant larvae to administer a novel mRNA-based therapy enclosed on lipidic nanoparticles produced by Ethris GmbH.

To come as close as possible to a viable treatment for human PCD patients, we tested a topical delivery in zebrafish larvae. Hence, zebrafish larvae were placed in zebrafish medium enriched with formulated LNPS with CCDC40 cmRNA at 30 hpf. The incubation period was tested (1 day, 2 days or 4 days of incubation) and two different mRNA concentrations of 10 and 20 ng/µL were investigated. We concluded that an increase in cilia beating frequency (CBF) was accomplished by incubating *ccdc40*$^{-/-}$ larvae for 4 days with LNPS formulated with CCDC40 cmRNA at 20 ng/µL. These conditions enabled a partial recovery of ciliary movement in small localized areas of the olfactory pit of the zebrafish. Our conclusions are that tests should continue to increase the concentration under the duration of 4 days of incubation with renewal of therapy at 2 days.

Key words: Motile Cilia, Primary ciliary dyskinesia (PCD), CCDC40, LNPs formulated with cmRNA, Zebrafish

Resumo

A discinesia ciliar primária (DCP) é uma doença genética causada pela inexistência ou mau funcionamento dos cílios móveis, responsáveis pela remoção do excesso de muco e bactérias das vias respiratórias. Indivíduos com DCP sofrem recorrentemente de infeções respiratórias e bronquiectasias. A DCP advém de mutações em vários genes responsáveis pela estrutura e função ciliar dos cílios móveis.

Neste projeto, foi necessário identificar mutantes de peixe-zebra, previamente criados usando CRISPR-Cas9, de forma a mimetizar mutações humanas na região homóloga do genoma do peixe-zebra, em 4 genes causadores de DCP: DNAH-5, DNAH-11, CCDC39 e CCNO. Sendo que não foi possível, no período dedicado ao meu projeto de Mestrado, identificar peixes homozigotas de nenhum dos genes selecionados, utilizámos mutantes F1 *ccdc40*$^{+/-}$ já identificados para gerar larvas homozigotas e para administrar uma terapia inovadora à base de mRNA incorporada em nanopartículas lipídicas produzidas pela empresa Ethris GmbH.

De forma a transpor este tratamento futuramente para doentes de DCP, testámos uma via de absorção tópica como forma de administrar a terapia às larvas de peixe-zebra. Desta forma, as larvas foram colocadas num meio enriquecido com as nanopartículas formuladas com mRNA CCDC40 a 30 hpf. Testámos o tempo de incubação (1 dia, 2 dias ou 4 dias de incubação) e duas concentrações distintas de mRNA (10 or 20 ng/µL). Percebemos que a frequência de batimento ciliar (FBC) apenas aumentou em larvas incubadas 4 dias com NPLs formuladas com mRNA a uma concentração de 20 ng/µL. Sob estas condições é possível haver recuperação do batimento dos cílios numa área reduzida do órgão olfativo do peixe-zebra. Estas conclusões sugerem que devem ser continuados testes aumentando a concentração de mRNA durante o período de incubação de 4 dias, com renovação da terapia aos 2 dias.

Palavras-Chave: Cílios Móveis, Discinésia Ciliar Primária (DCP), CCDC40, Nanopartículas formuladas com mRNA, Peixe-Zebra

Contents

List of abbreviations

aa – Amino acid
ATP - Adenosine triphosphate
CBF - Cilia beating frequency
CCDC39/40 - Coiled-coil domain containing protein 39/40
CCNO - Cyclin O
cmRNA - chemical modified ribonucleic acid
CRISPR-Cas9 - Clustered regularly interspaced short palindromic repeats associated with caspase 9
gDNA – Genomic deoxyribonucleic acid
DNAH5/11 - Dynein axonemal heavy chain 5/11
dpf - days post-fertilization
GFP – Green fluorescent protein
hpf - hours post-fertilization
HTD - Heteroduplex
HVMA - High-speed video microscopy analysis
IDA - Inner dynein arm
IFT - Intraflagellar transport
Indel – insertion/deletion
LNP - lipidoid nanoparticle
MTOC - Microtubule organizing center
N-DRC - nexin-dynein regulatory complex
NCBI – National Center for biotechnology information
ODA - Outer dynein arm
ON - overnight
OP - olfactory pit
PAGE - polyacrylamide gel eletrophoresis
PAM – Protospacer adjacent motif
PCD - Primary Ciliary Dyskinesia
PCR – Polymerase chain reaction
PIV - Particle Image velocimetry
RS - Radial spoke
ROI – Region of interest
sgRNA - short guide ribonucleic acid
SNIM®RNA - Stabilized Non-Immunogenic mRNA
TEM - Transmission electron microscopy
Tg - Transgenic
WT - Wildtype

List of Figures

List of Tables

List of Videos

Supplemental video 1 – Example of a high-speed video microscopy of beating cilia in the olfactory pit of a 5 day old *ccdc40*$^{-/-}$ zebrafish larvae after 4 day incubation with formulated LNPs containing 20 ng/µL of cmRNA of CCDC40, related to Figure 21 C.

Supplemental video 2 – Example of a high-speed video microscopy of beating cilia in the olfactory pit of a 5 day old *ccdc40*$^{-/-}$ zebrafish larvae after 4 day incubation with formulated LNPs containing 20 ng/µL of cmRNA of CCDC40, related to Figure 21 C.

Supplemental video 3 – Example of a high-speed video microscopy of beating cilia in the olfactory pit of a 5 day old *ccdc40*$^{-/-}$ zebrafish larvae after 4 day incubation with formulated LNPs containing 20 ng/µL of cmRNA of CCDC40, related to Figure 21 C.

Supplemental video 4 – Example of a high-speed video microscopy of beating cilia in the olfactory pit of a 5 day old *ccdc40*$^{-/-}$ zebrafish larvae, related to Figure 21 C.

Supplemental video 5 – Example of a high-speed video microscopy of beating cilia in the olfactory pit of a 5 day old *ccdc40*$^{-/-}$ zebrafish larvae, related to Figure 21 C.

Supplemental video 6 – Example of a high-speed video microscopy of beating cilia in the olfactory pit of a 5 day old *ccdc40*$^{-/-}$ zebrafish larvae, related to Figure 21 C.

Supplemental video 7 – Example of a high-speed video microscopy of beating cilia in the olfactory pit of a 5 day old *ccdc40*$^{+/-}$ sibling zebrafish larvae, related to Figure 21 C.

Supplemental video 8 – Example of a high-speed video microscopy of beating cilia in the olfactory pit of a 5 day old *ccdc40*$^{+/-}$ sibling zebrafish larvae, related to Figure 21 C.

Supplemental video 9 – Example of a high-speed video microscopy of beating cilia in the olfactory pit of a 5 day old *ccdc40*$^{+/-}$ sibling zebrafish larvae, related to Figure 21 C.

1. Introduction

1.1. Cilia origin

Antoine Van Leeuwenhoek, a Dutch scientist pioneer in microscopy, first described the existence of “microscopic creatures” with “tiny legs” swimming in a droplet of rainwater, in 1676[53]. Van Leeuwenhoek observations were only possible due to his simple microscope work, which surpassed the capabilities of the compound microscopes of his era. Hence, these innovative instruments enabled the observation of life forms, previously invisible to human eye[52]. However, at that time, their biological significance was not fully understood.

Cilia, along with flagella, are believed to have originated in some of the earliest single-celled organisms[66]. These microorganisms, such as protists, possessed rudimentary cilia-like structures that helped the navigation through their aqueous environment and capture of nutrients. Over time, cilia underwent substantial adaptations and refinements, becoming a ubiquitous feature not only present in simple protozoa, but also in complex multicellular animals, including humans.

The origin of cilia seemed to be traced to the need for efficient locomotion and sensory perception in those early life forms. However, cilia followed the development of organisms and evolved to serve a multitude of functions beyond movement. Nowadays, their contribution to diverse processes such as propulsion of sperm cells or movement of mucus in the respiratory tract is already unravelled[66].

Ultimately, research concerning cilia is a collaborative effort spanning for four centuries, with a variety of contributions from scientists across different fields. It has been driven by the continuous advancement of microscopy and molecular biology techniques. This collective effort has deepened the understanding of cilia’s structure and functions in various organisms.

1.2. Cilia structure and function

The exploration of cilia structure began with the introduction of electron microscopy in the mid-1950s, enabling the visualization of cilia at a level of detail previously unattainable, revealing their complex internal structure[99].

Our current understanding of ciliary biology has emerged from studies conducted in unicellular models, including green *algae* such as *Chlamydomonas reinhardtii* or protozoa like *Tetrahymena termophila*. These studies have provided invaluable insights into the complexity and evolutionary conservation of ciliogenesis. Moreover, it has become clear that this process involves over 300 different proteins, along with specific requirements for achieving ciliary motility[39,81].

Cilia are hair-like structures, highly conserved, that protrude from the cell's plasma membrane. They are built during cellular differentiation and reabsorbed when the cell re-enters the cell cycle[89]. The main compartments of a cilium consist of a basal body, a transition zone, the axoneme and a ciliary tip (Figure 1 A)[66,108].

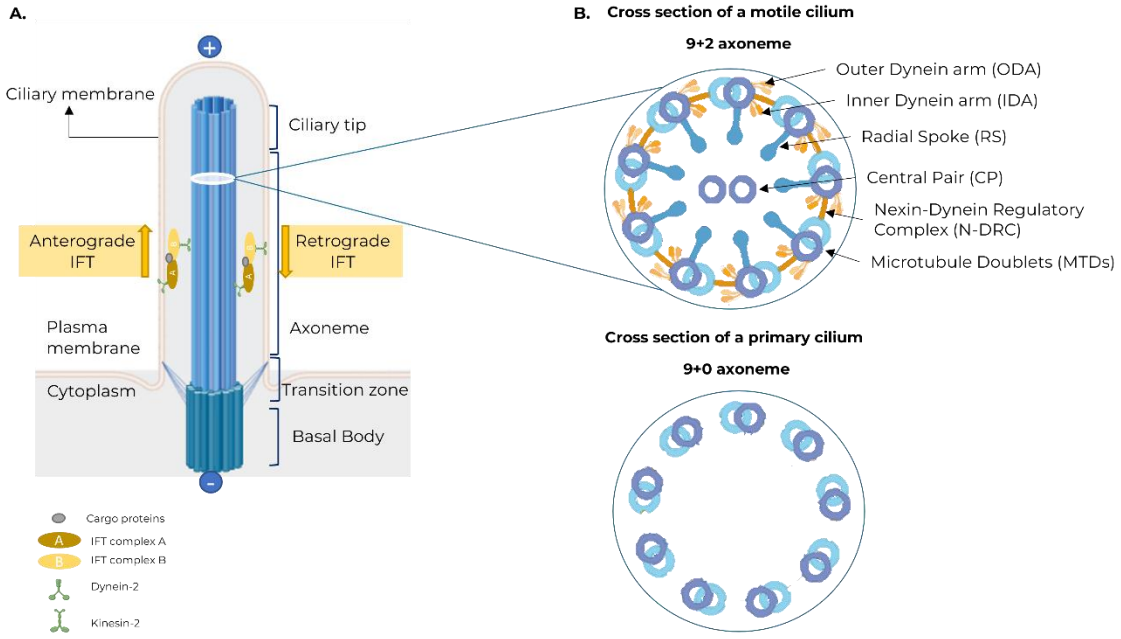

Figure 1 - Ciliary structure. *A) Schematic diagram of the ciliary axoneme. It consists of four principal components: basal body, transition zone, axoneme and ciliary tip. Ciliary components are transported along the axoneme by intraflagellar transport (IFT) that includes anterograde and retrograde movements. This transport is driven by kinesin and dynein motors. B) Transversal view of the axoneme organization in a motile (9+2) and non-motile (9+0). Adapted from Yan, L et al 2022*[115].

To build cilia, two similar proteins are required: α-tubulin and β-tubulin[14,36]. These two proteins combine to form dimers, which subsequently assemble into a polymer. Then, this polymer coils into a tube, forming a track for intraflagellar transport (IFT) [48,95]. The base of the microtubule is firmly anchored to the microtubule organizing center (MTOC), originating from the centriole. The opposite end remains unattached, allowing for the addition or removal of tubulin dimers in response to the cell's requirements (Figure 1 A).

A cilium operates independently from the cytoplasm. However, all the building blocks needed for its assembly are produced within the cytoplasm and then selectively transported from the minus end, through the transition zone, to the plus end of the cilium. The assembly of cilia follows a bottom-to-top pattern, with new proteins being transported to the ciliary tip. Furthermore, when it becomes necessary to disassemble the cilia, all these components must return to the cytoplasm.

In addition to these building blocks, motor proteins also facilitate the bidirectional transport of signalling molecules. Kinesin-2 is responsible for anterograde movement whereas cytoplasmic dynein-2 oversees ciliary retrograde movement, shuttling cargo in and out of the cilia, respectively[48,70]. In humans, there are 46 identified kinesins[65] and 17 cytoplasmic dyneins[32], each possessing distinct motor domains tailored for specific types of transportation. However, in the cilium only kinesin-2 and dynein-2 are present[109].

The distal tail domains of these motor proteins selectively bind to cargo, while their motor domains interact with microtubules. These motor domains have the capability of hydrolysing adenosine triphosphate (ATP), using the energy generated to move forward along the microtubule[94]. Hence, when these motor proteins are lacking, the cilia are not correctly assembled or show length and morphology defects[109].

There are two main types of cilia: non-motile, or primary, cilia and motile cilia. Non-motile cilia are ubiquitous among most cell types in the human body. However, they lack the central pair and axonemal dynein arms, having a 9+0 conformation (Figure 1 B). Consequently, they do not have the beating capability and seem to be shorter than motile cilia. Instead, primary cilia are mostly associated with sensory perception and cell signalling. They contain various receptors and are involved in processes like signal transduction and cell communication[9,114]. Nonetheless, there are 9+0 cilia that can possess dynein arms and, subsequently, display beating capabilities like for example droshophila chordotonal neurons cilia[43].

On the other hand, motile cilia are usually found on the surface of certain types of cells such as those lining the respiratory tract, fallopian tubes, and the ventricles of the brain. They exhibit a 200 nm diameter cytoskeletal stack with a characteristic 9+2 microtubule structure which consists of nine doublet microtubules linked by nexin fibers surrounding a central pair (Figure 1 B)[108]. This arrangement, enclosed in

a ciliary membrane, provides structural support, and allows for movement due to the existence of dynein arms. Each doublet has two tubules, one complete (A) and other incomplete (B).

Microtubule A has two dynein arms attached: the inner dynein arm (IDA) and the outer dynein arm (ODA)[27]. The IDA and ODA consist of axonemal dynein proteins that can differ by having DNAH (heavy chains), DNAI (intermediate chains), and DNAL (light chains). While IDAs are thought to fulfill various functions in ciliary motility, including initiating bend formation along the microtubule, the ODAs are large protein complexes comprising heavy (400-500 kDa), intermediate (45-110 kDa) and light (8-55 kDa) dynein chains[39,47]. ODAs are believed to play a significant role in providing power stroke necessary for microtubular curvature[39,57]. These proteins hydrolyse ATP, transforming it into kinetic energy. When IDA and ODA contact with the B microtubule, it is induced a sliding motion between the doubles that powers the axoneme and consequently cause a specific pattern[44,86]. According to NCBI database, there are 12 dynein proteins composing ODAs and 15 dynein proteins in IDA in humans.

Motile cilia also have nexin links, components identified as part of the dynein regulatory complex (N-DRC). Besides maintaining microtubule integrity, N-DRC also influence axonemal bending by regulating the IDAs connection to the microtubule A, thus facilitating communication between the central pair and the dynein arms through the radial spoke (RS)[58,118]. Additionally, the coordinated beating of cilia are essential, among others, for the circulation of cerebrospinal fluid, reproductive system function, and maintaining respiratory system homeostasis. Cilia also have a role linked to the sense of olfaction[72]. The rapid replacement of odour molecules with new ones enables our nose to relay the most current environmental signals to the brain[1].

Furthermore, even though motile cilia share a conserved macro-structure, variations in cilia beating frequencies and patterns can occur due to specific factors like ciliary ultrastructure and cilia length[84,97,108].

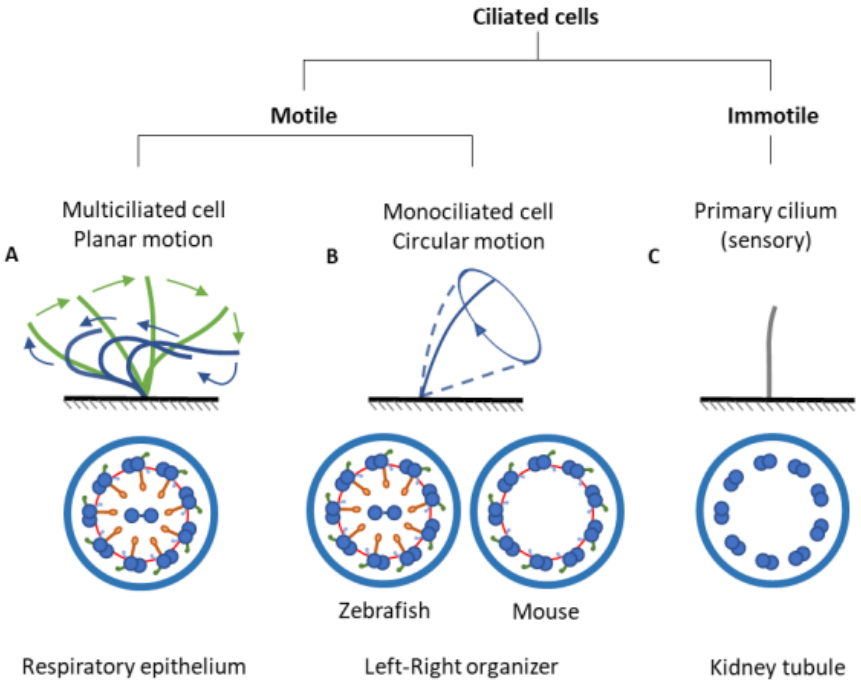

Figure 2 - Diversity of cilia types and movement in vertebrates. *Examples of a respiratory motile cilium, a motile cilium from left-righ organizer and a primary kidney cilium are depicted. For each example, a representation of the ultrastructure of a transversal view of the cilium is shown. A) Human airway cilia present a 9+2 microtubular structure, exhibiting a planar asymmetric motion due to uneven cilium bending. B) Cilia from the LRO exhibit a counterclockwise circular movement. C) Primarry immotile cilia of kidney epithelial cells, acting as a sensory cilium. Adapted from Sampaio, P*[91].

Specifically in the human respiratory cilia, characterized by a 9+2 axoneme arrangement, their motion exhibits a distinct planar beating stroke (green) followed by a recovery stroke (blue) (Figure 2A). During this process, an asymmetric bending of the cilia between two strokes generates a propelling effect on the mucous layer. Therefore, the coordinated activity of mutiple cilia beating with a constant phase difference between adjacent neighbours initiates a metachronal pushing wave[100]. This synchronized and rhythmic beating of cilia, which can be as dense as 200 per cell, is crucial for the self-clearing mechanism of the airways, commonly referred to as mucociliary clearance[105].

Altogether, if any ciliary components are compromised cilia related disorders emerge due to cilia dysmotility.

1.3. Ciliopathies

Characterized by dysfunctional or structural abnormalities in cilia, ciliopathies result from mutations in genes responsible for the formation and maintenance of cilia. These hair-like structures protrudes from the surface of most cells throughout

the human body and when affected may lead to a wide range of clinical manifestations, compromising various organs and systems within the body.

Primary cilia play crucial roles in sensing and transmitting signals during development, tissue maintenance, and response to external stimuli[114]. Among other functions, cilia serve as antennae capturing signalling molecules. Additionally, primary cilia respond to stimuli such as light and odours in the eye and olfactory epithelium, detect fluid flow within the kidney, and sense pressure within bone tissue[27].

When it comes to diagnosing ciliopathies, it may be a major challenge since these diseases can exhibit both variable and overlapping symptoms. Because of this, finding appropriate treatment is also difficult. Depending on the affected genes and the specific primary cilia functions disrupted, ciliopathies can manifest as a spectrum of disorders such as polycystic kidney disease, Bardet-Biedl syndrome, Joubert syndrome, among others[5]. Multiple systems are often jeopardized in these conditions including eyes, liver, brain, kidneys, and lungs.

1.4. Primary Ciliary Dyskinesia

Appart from the syndromic ciliopathies, there is a particular ciliary disease named primary ciliary dyskinesia (PCD). PCD is predominantly an autosomal recessive genetic disorder, having a prevalence of 1:10 000 to 1:20 000 live-born children[54,69,104].

This condition is known for affecting specifically the structure and function of motile cilia present in cells of the respiratory epithelium, for instance. In order to clear the respiratory tract, cilia have to be appropriately coordinated, making the mucus and other substances to move, facilitating the proper function of the respiratory and reproductive systems for example.

In PCD patients, there is a defect in the structure or movement of cilia, leading to cilia dysfunction in respiratory cells. Consequently, the effective removal of mucus, bacteria and other particles by cilia is compromised. As a result, individuals with PCD often experience chronic respiratory problems, including recurrent sinus infections, chronic wet cough, and frequent lung infections such as bronchiectasis due to opportunistic colonization of bacterial agents[46]. Additionally, PCD may also involve infertility, hydrocephaly, and *situs inversus* due to the presence of motile cilia in sperm, oviducts, ependymal cells lining the brain ventricles, and epithelial cells in the left-right organizer during embryogenesis, respectively[23].

Concerning PCD diagnosis, it is important to do it in early stages and intervene right away to improve the quality of life of PCD patients and monitor the disease. However, this seems to be a challenge since this disease is still under-diagnosed or has a delayed confirmation[50,51]. This can be attributed to the lack of awareness, shortage of experienced personnel or absence of specialized equipment required for accurate assessments[20]. Hence, European guidelines recommend the use of a multidisciplinary diagnostic pipeline including nasal nitric oxide measurement, high-speed video microscopy analysis (HVMA), transmission electron microscopy (TEM), ciliary protein immunofluorescence and genetic screening[62,103].

Although there is yet no treatment for PCD, the focus is to help relieve symptoms and limit the progression of potential complications like bronchiectasis. This typically involves taking antibiotics to manage infections supplemented with chest physiotherapy to help clear mucus from the airways[6,21,31]. In extreme cases of bronchiectasis and infection, lobotomy can be considered or even lung transplantation[110].

Research into understanding the genetic basis of PCD and developing effective treatments is ongoing, with the aim of improving outcomes and quality of life for those affected by this complex and challenging disease.

1.5. PCD causing genes

To date, over 50 distinct genes were reported as contributors to PCD (MIM 244400)[111]. These genes encompass various anomalies such as defects in ODAs[76], IDAs, nexin links, central apparatus, or RS[102]. In some cases, gene mutations impact the pre-assembly and maturation of dynein complexes, resulting in simultaneous malfunctions of both ODAs and IDAs[102].

Approximately 25% of all cases of PCD can be attributed to mutations in DNAH1, DNAH5 and DNAH11 genes[82]. Nonetheless, a malfunction in any of the other 120 proteins involved in cilia structure or in cytoplasmic proteins responsible for constructing ciliary components has the potential to disrupt cilia ultrastructure, which reflects on a spectrum of effects, ranging from partial to complete loss of ciliary motility[78]. These effects comprise alterations in the pattern of ciliary beating[92] or in sporadic cases an increase in beat frequency combined with a restricted range of motion[101]. Figure 3 illustrates the most frequently mutated genes and the respective impact on the axoneme structure of cilia.

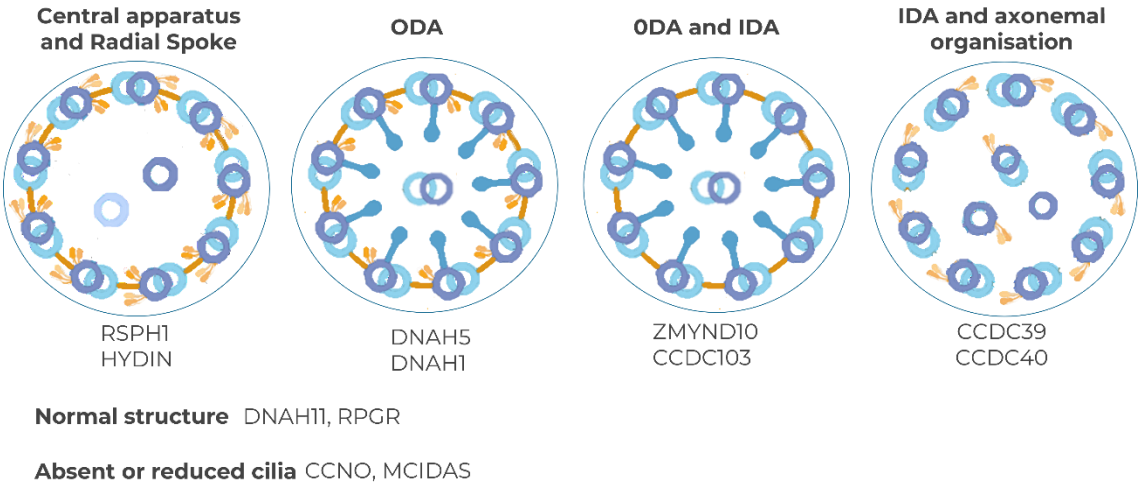

Figure 3 - Typical axoneme defects in different mutated genes in PCD. *List of some PCD-related genes that when mutated reveal absence of certain components like ODA, IDA or central pair. Axoneme disorganization can also occur. There are two identified genes that when mutated impair cilia formation. Adapted from Ferkol, 2017*[26].

PCD genes selected in this study

Here, I will briefly characterize a number of PCD genes that we first selected to generate zebrafish animal models.

CCNO gene

The CCNO gene, which stands for "Cyclin O" encodes a protein, member of the cyclin protein family, that plays a role in cell cycle regulation. Cyclins are proteins that help control the progression of the cell cycle, ensuring that cell division occurs at the right time and under proper regulation. Cyclin O is specifically required for generation of multiciliated cells, potentially by promoting a cell cycle phase compatible with the proliferation and development of centrioles[110].

In respiratory cells, CCNO localizes within the apical cytoplasm of multiciliated cells and plays an important role during the amplification and migration of basal bodies[12,110]. CCNO not only facilitates centriole assembly in multiciliated cells, preparing them to their critical role in apical docking[110], but also increases the number of mother centrioles when overexpressed during multiciliated cell differentiation.

Even though, CCNO mutations do not cause complete absence of multiple motile cilia, there is a significant reduction in their number due to defects in mother centriole generation and migration during multiciliated cell differentiation. Additionaly, cilia tend to be shorter and exhibiting no movement[18]. As a consequence, this can be referred as a congenital mucociliary clearence disorder with reduced generation of multiple motile cilia. However, mutations in CCNO do not affect the localization of motility-related proteins within the cilium, such as DNAH5 and CCDC39[110].

Even though the prevalence of CCNO mutations in PCD is exceptionally low, with an incidence rate lower than 2% in all identified PCD patients, new reports of this mutation are being published[106]. In our diagnostic service in Lisbon we have identified already 3 patients with mutations in CCNO. They all presented early-onset respiratory symptoms, including obstructive ventilatory impairment, followed by a period of relative stability. Additionally, transmission elctron miscroscopy and high-speed video microscopy analysis revealed a reduced number of cilia with uncoordinated beat pattern, even tough the axoneme ultrastructure was normal[34].

In the human genome, CCNO is located on chromosome 5 (ENSG00000152669) and has 2 identified transcripts, with only one known to produce a functional protein. In zebrafish, *ccno* gene is located on chromosome 5 (ENSDARG00000099542), has only one transcript annotated that can result into a protein.

DNAH5 and DNAH11 genes

Axonemal dyneins are molecular motors particularly important for enabling cilia movement[44]. They are responsible for generating bending and waving movements by using energy derived from the hydrolysis of ATP. For this to happen, multiple dynein arms present along the axoneme must have a coordinated action[86].

Outer dynein arms (ODAs) are composed by various chains of axonemal dyneins within ciliary microtubular structures found in respiratory epithelia. ODAs structure is composed by a spherical head domain that consists of γ-type and β-type heavy chains. This section is linked to intermediate dynein chains which are subsequently linked to light chains. Together with a docking subunit, this complex of dynein chains is anchored to the A-microtubules[35,73]. Two distinct types of ODAs have been reported in human respiratory cells. According to the composition of their dynein heavy chains they can be identified as type 1 or type 2 ODAs. Type 1 ODAs are situated in the proximal region of the cilia and consist of dynein axonemal heavy chain 5

(DNAH5) (γ -type) and dynein axonemal heavy chain 11 (DNAH11) (β-type), whereas type 2 ODAs are found in the distal part of the cilia and are composed of DNAH5 (γ -type) and dynein axonemal heavy chain 9 (DNAH9) (β-type)[25,28]. The ODA multiprotein complex is responsible for providing the energy required to facilitate the bending motion of motile cilia[29].

The most commonly observed motile cilia defects in PCD patients involve the dynein arms, particularly ODAs, either affecting their assembly, anchory or structure[62,67]. Thus, absence of ODAs, or even simultaneous loss of both ODAs and IDAs[111] affects approximately 70% of individuals diagnosed with PCD[62,74,80].

The most common genetic defect observed in PCD are mutations in DNAH5 enconding axonemal ODA heavy chain 5[37], resulting in partial or complete loss of the total ODA complex, consequently leading to complete immotile cilia or possibly exhibiting only minimal residual movements[76].

Mutations in DNAH11, another ODA that is very commonly mutated in Asia[83], are associated with a normal 9+2 axonemal ultrastructure[7,45,101]. However, cilia display a characteristic hyperkinetic ciliary beating with reduced amplitude. DNAH11 mutations can also be detected by immunofluorescence[60].

In the human genome, DNAH11 is located on chromosome 7 (ENSG00000105877) and has 10 identified transcripts, with at least 2 known to produce a functional protein. Whereas, DNAH5 is located on chromosome 5 (ENSG00000039139) and has 14 identified transcripts, with at least 2 known to produce functional proteins. In zebrafish, *dnah11* is located on chromosome 16 (ENSDARG00000094282), has only two transcripts annotated and both can result into proteins. Likewise, *dnah5*, located on chromosome 16 (ENSDARG00000087373), also has two transcripts annotated that can result into proteins.

CCDC40 and CCDC39 genes

One of the genes that underlies most severe forms of PCD encodes a protein known as Coiled-Coil Domain-containing protein 40 (CCDC40) (HGNC:26090)[10,107].

CCDC40 is responsible for the correct assembly of the N-DRC and IDAs,[8,64,75] as well as the RS attachment to the A-tubule[4,113]. Hence, it is a crucial element in the axonemal spatial integrity. Futhermore, seems like CCDC40 also participates in tubulin polyglutamylation at the proximal end of the cilium[56]. It is believed that this post-translational modification regulates microtubule stability[49].

Likewise, Coiled-Coil Domain Containing protein 39 (CCDC39) encodes a protein that is part of the ciliary axoneme. This protein is also necessary for the correct assembly of dynein regulatory complex, as well as IDA assembly, consequently regulating ciliary beat.

These two proteins form an integral part of the motile cilia molecular ruler complex. This complex plays a role in ensuring the precise repetition of the fundamental ciliary structure every 96 nm along the axoneme[75]. This molecular ruler acts as a signaling mechanism, indicating the precise attachment sites of the radial spokes (RS) along the axoneme. Additionally, it facilitates the anchoring of the IDA and the N-DRC to the neighbouring doublets of the axoneme[8]. When this complex is absent, there is an impaired number of RS binding the A-tubule. This results in extreme disorder of the ultrastructure of cilia, leading to what are known as axonemal ruler defects. This combines absence of IDAs, doublet translocations to the centre, and acentric or absent central pairs likely resulting from the deficient assembly of N-DRC[4]. Consequently, this disruption adversely affects ciliary motility.

In this specific case, individual CCDC39 or CCDC40 mutations result in similar defects that generate indistinguishable ultrastructural phenotypes[10]. The prognosis of individuals who harbor these mutations tends to be worse compared to PCD patients with mutations in other genes[22]. Even tough there is not a clear reason for this event, patients often suffer from more severe symptoms such as higher neonatal respiratory distress and lower forced expiratory volume as well as an overall poorer condition (lower body mass index). It was noticed that the existence of these mutations, do not completely abolish cilia movement. Instead, cilia beating is faster in a flickering way, with very low amplitude[17].

CCDC40 has been identified in various organisms. According to AmiGO2 database, it is situated within cilia (including respiratory epithelia, sperm flagella, and the primary cilium of the left-right organizer). In the human genome, CCDC40 is located on chromosome 17 (ENSG00000141519) and has 16 identified transcripts, with at least 7 known to produce a functional protein. Whereas CCDC39 is located on chromosome 3 (ENSG00000284862) and has 11 identified transcripts, with at least 4 known to produce a functional protein. In zebrafish, *ccdc40* is located on chromosome 6 (ENSDARG00000100584), has only two transcripts annotated with only one resulting in a functional protein. Zebrafish *ccdc39* is located on chromosome 2 (ENSDARG0000010091), has only two transcripts annotated and both can result into functional proteins.

1.6. CRISPR-Cas9 as a gene editing tool

The clustered regularly-interspaced short palindrominc repeats associated with Caspase 9, simply known as CRISPR-Cas9, is a revolutionary gene editing technology that allows the modification of genes in a precise and targeted manner.

This method reports to the defence mechanism developed by bacteria to combat invading pathogens like viral infections[11,68]. It is essentially a genetic memory system of bacteria. When infected by virus, bacteria are capable of storing a portion of viral DNA (spacer) in between the PAM (Protospacer adjacent motif) sequences[11]. Upon a subsequent viral encounter, the bacteria generates two distinct types of RNA. One is crRNA, which stands for CRISPR RNA, that carries a sequence that complements the spacer. The other is tracrRNA (trans-activating crRNA), responsible for the connection between crRNA and Cas9[24]. These two molecules form a complex with Cas9, which functions as both helicase and nuclease. When this complex identifies a sequence that matches the crRNA, Cas9 induces a double-stranded break (DBS) in the DNA, effectively neutralizing the virus.

Transposing this system to human cells, there are multiple types of CRISPR-Cas systems[63]. However, type II, using Cas9 is most used in genetic manipulation. Scientists adapted it to be able to cut any DNA strand at a specific site by changing the sequence in the guide RNA (combination of crRNA and tracrRNA) as long as it is followed by a PAM sequence[42].

The canonical PAM sequence comprises a 5'-NGG-3' pattern, with "N" representing any base, and its commonly found within the genome[3]. Consequently, the CRISPR-Cas9 system can potentially cut any site within the genome. However, the requirement for recognizing the PAM by Cas9 imposes limitations on targeting and has an impact on editing efficiency[30]. Thus, other PAM sequences, called non-canonical, have been studied to remove this limitation, namely 5'-NGN-3'[112] and 5'-NNG-3'[59] sequences.

The short guide RNA (sgRNA) consists of a small pre-designed RNA sequence (about 20 bases long) located within a longer RNA scaffold. It is designed to find and bind to a specific sequence in the DNA (PAM). The sgRNA has RNA bases complementary to those of the target DNA sequence in the genome. Thus, teoretically, the sgRNA will only bind to the target sequence and no other regions of the genome (Figure 4).

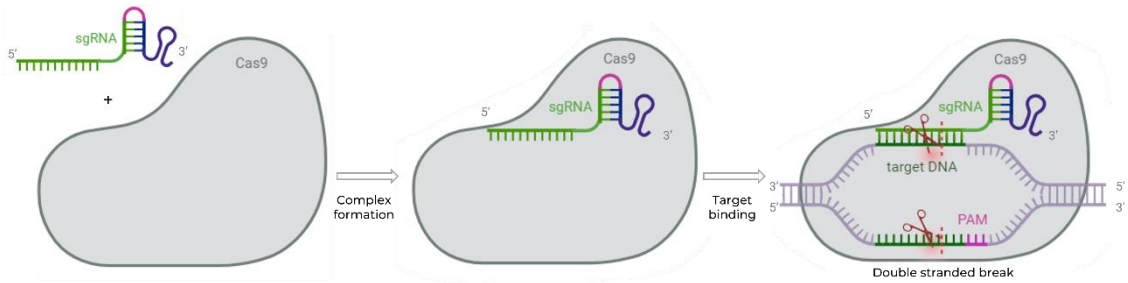

Figure 4 - CRISPR-Cas9 system. *Formation of the short guide and Cas9 complex followed by binding of this complex to target DNA, inducing Cas9 to break the double strand DNA.*

The sgRNA can be injected into a cell or an embryo together with Cas9 mRNA or Cas9 protein itself. Once inside the nucleus, the complex sgRNA-Cas9 anchors to the PAM. Next, Cas9 unfolds the DNA strands and aligns them with the target sequence in the sgRNA. If a successful match is achieved, Cas9 induces a DSB in the DNA. The cell recognizes that DNA is damaged and tries to repair it. In eukaryotes, the most common approach is the non-homologous end joining (NHEJ). It earns its name because it doesn't rely on a template. Rather than using a template, the repairing enzymatic complex modifies the broken ends by either removing or adding bases, subsequently rejoining the resulting extremities[55]. As a result, this process is prone to error resulting in random base insertions, deletions or frameshift mutations that can silence the gene. However, this system also creates a potential to substitute a mutated gene with a healthy version. Following the homology-directed repair pathway, it is introduced a DNA sequence containing the correct genetic code (called template) alongside the sgRNA and Cas9[40]. When Cas9 cuts the DNA, the cell uses the given DNA template during the repair process, facilitating the exchange of nucleotide sequences and proficiently filling in the gaps without introducing errors[13] (Figure 5).

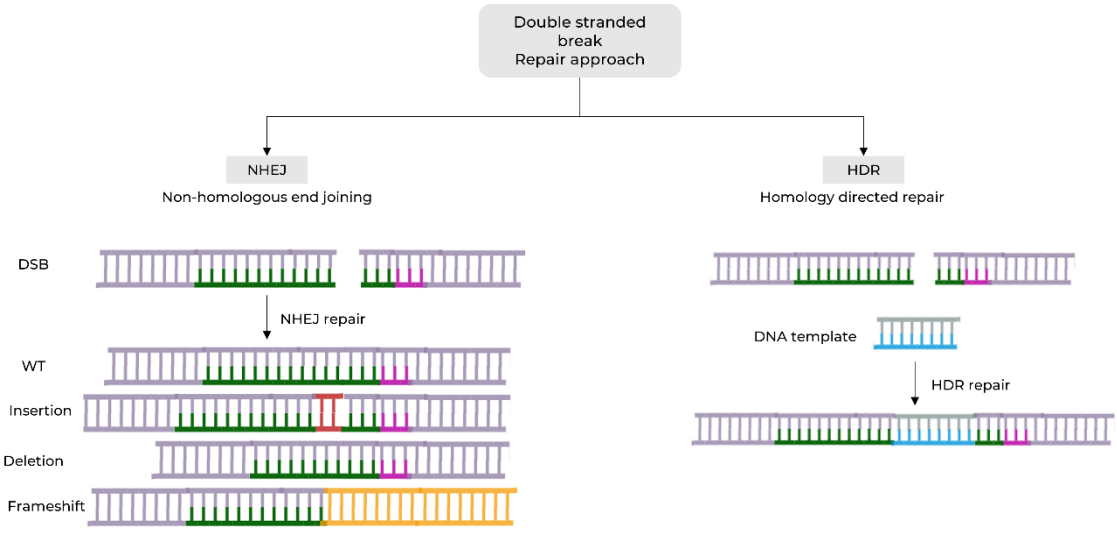

Figure 5 – Repair approaches of double stranded break (DSB) caused by CRISPR-Cas9. *After de Cas9 makes a DSB, the cell can repair the cut by either Non-homologous end joining (NHEJ) or Homology directed repair (HDR).*

In summary, CRISPR-Cas9 technique is currently the simplest, fastest, cheapest, most versatile and precise method, when compared to other genetic manipulation tools like TALENS (Transcription activator-like effector nucleases) or ZFNs (Zinc-finger nucleases). It can be used for gene knockdown, enabling the investigation of a gene's function within a cell or organism.

1.7. Zebrafish as an animal model

Zebrafish (*Danio rerio*) possess several characteristics that make them an extremely helpful tool for scientific research, ranging from developmental biology to genetics, neuroscience, toxicology, and even regenerative medicine[19,85].

The zebrafish is a vertebrate that has an exterior fertilization which means that the embryos develop outside the mother's body, allowing researchers to observe and manipulate its developmental processes. In addition, zebrafish development is a fast process, having the ability to produce a large number of eggs that experience significant developmental landmarks within some days, which expedites the pace of research and experimentation. On top of that, zebrafish also has the ability to regenerate tissues and organs[19].

Zebrafish, by their inherent nature, lack lungs. However, they possess an olfactory pit (OP) with a multiciliated epithelium, identical to the one found in humans[85,93]. The OP, situated between the eyes in zebrafish, is a bilateral sensory organ that becomes visible at approximately 30 hous post fertilization (hpf), reavealing its surface[33]. This

organ takes on a cup-like structure and its base is filled with olfactory receptor neurons, each presenting non-motile cilia with olfactory receptors. Additionally, the periphery is lined by a layer of multiciliated cells with motile cilia that are visible at 5 dpf[72]. Because of its structural resemblance to the human respiratory epithelium and its accessability, the larval OP represents a significant organ of interest for the investigation of PCD[85]. Furthermore, due to its small size, zebrafish larvae are adequate for therapy bathing, optimizing and economizing the use of liquid with nanoparticles formulated with mRNA to conserve this valuable resource.

Moreover, researchers can easily genetically modify the zebrafish genes due to their relatively simple and well annotated genome, which shares many genes with humans. Among all the genes identified in the human genome, approximately 70% have a corresponding homologous gene within the zebrafish genome[38,85]. Gene editing techniques like CRISPR-Cas9 can be used by researchers to introduce mutations in targeted genes, allowing them to explore roles of several genes in development and disease and further test new lines of treatment. Pinto et al. 2021 presents in a summarized way Human-Zebrafish homologue PCD genes according to Ensembl genome browser, demonstrating that almost all PCD human genes show homologous genes in zebrafish[85].

For instance, the *ccdc40*$^{-/-}$ mutants have cilia exhibiting axonemal ultrastructural disarrangements similar to those observed in humans. This loss of motility inevitably leads to a functional impairment in maintaining a consistent water flow in and out the OP identical to how cilia in the respiratory tract fail to participate in mucociliary clearence in PCD patients. Given that, the ccdc40 mutant becomes an asset to study novel therapies for PCD.

Altogether, zebrafish presents many advantages over other animal models due to their rapid development, genetic tractability and ease of husbandry when compared to mice for instance. The many zebrafish contributions ultimately benefit human health and advancing biomedical knowledge[19].

1.8. Objectives

Patients with Primary Ciliary Dyskinesia have no curative treatment. This Master project is part of a larger project that represents a preclinical study using zebrafish as a model to test mRNA therapies for PCD.

The goals of this project are to:

a) Identify mutant carriers (F1) for previously injected zebrafish eggs (F0) with *dnah5*, *dnah11*, *ccno and ccdc39* short guide RNAs and Cas9 protein.
b) Test different dose-concentrations for *ccdc40* mRNA therapy delivery into ccdc40 mutants (F2).
c) Test different incubation periods per dose-concentration for *ccdc40* mRNA therapy delivery into ccdc40 mutants (F2).

2. Materials and Methods

2.1. Zebrafish housing and husbandry

All zebrafish used in this work were kept either at the CEDOC or IMM fish facility under controlled conditions approved by the Direção Geral de Alimentação e Veterinária (DGAV).

Adult zebrafish were kept in freshwater (28°C, 795 µS, pH 7) under a 14:10h light:dark cycle and fed with artemia and dry food. Embryos were obtained by natural mating and incubated at 28°C until 5 dpf, after which they were transferred to a tank in the main system or sacrificed following the current regulations.

Natural mating was stimulated by placing a male and one or two females inside a mating box in the evening. This mating box had a sieve to prevent the zebrafish from eating the eggs. Once the external fertilization of the eggs occurred, the adult zebrafish were returned to the main system tank. The eggs were collected by filtering the remaining water in the mating box and then placing them in a petri dish immersed in embryonic medium (5 mM NaCl, 0.2 mM KCl, 0.3 mM $CaCl_2$, 0.3 mM $MgSO_4$, and distilled water H_20, pH 6.5). The embryonic medium (E3) was renewed daily, and dead embryos were removed to prevent bacterial and fungal infections.

Larvae with 5 dpf were sacrificed by placing them in a bleach solution of 50%. Larvae older than 5 dpf and adult zebrafish were euthanized with tricaine (MS-222) at a 250 mg/L concentration.

2.2. Identifying Mutants

In August 2022, four different mutant zebrafish lines have been attempted using the CRISPR-Cas9 method to establish genotypes resembling those observed in humans with PCD. This approach was adopted to devise a more appropriate study protocol for investigating the genes implicated in PCD. This was performed by adjusting a previously published protocol[2]. The process is summarised in Figure 6 and further described in the following pages.

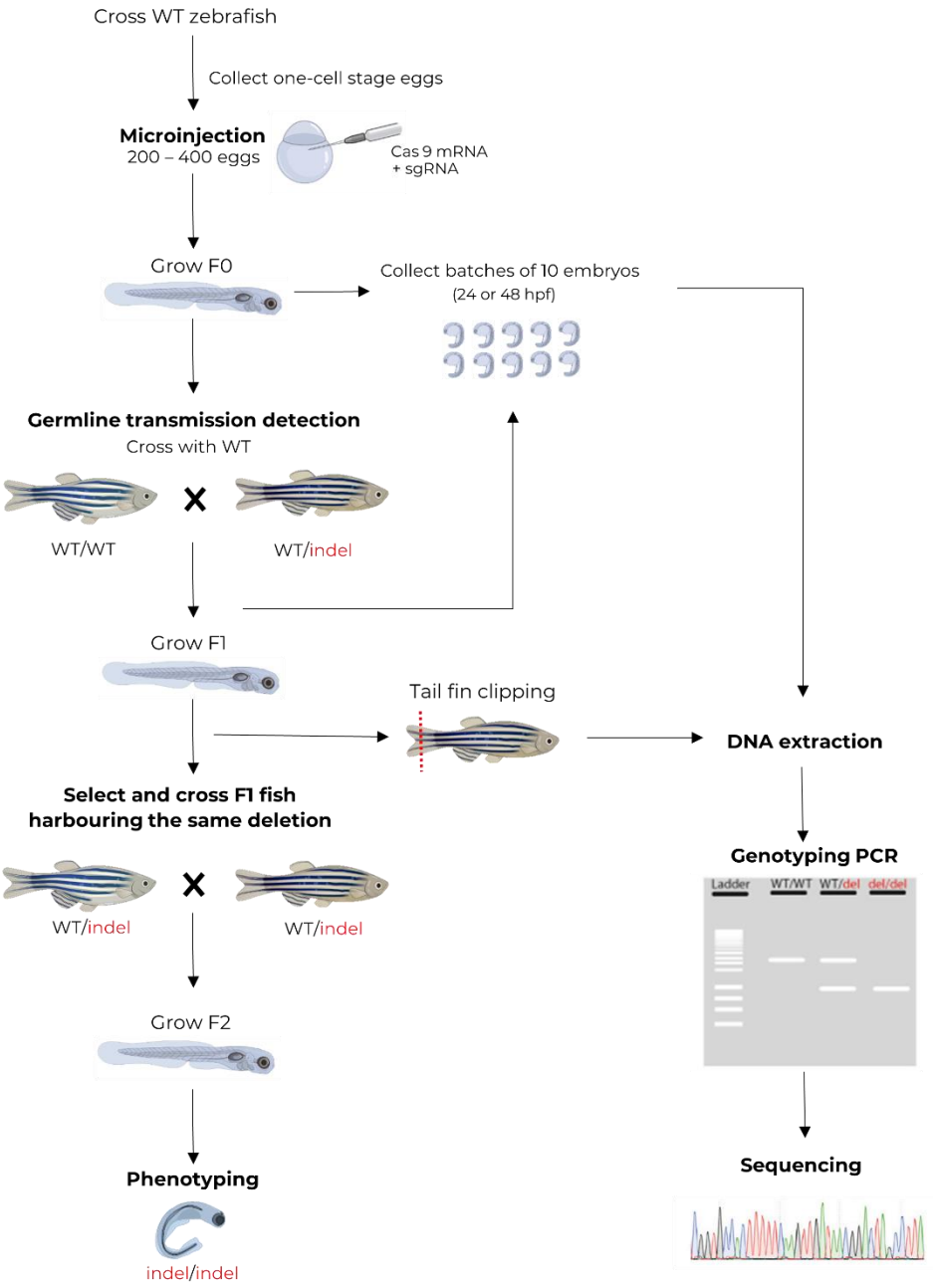

***Figure 6 - Pipeline from microinjection to establish a zebrafish mutant line**, adapted from Amorim et al, 2020[2].*

2.2.1. Micro co-injection of Cas9 mRNA and sgRNA

Multiple sg mRNA of different genes were injected separately into wildtype (WT) zebrafish, along with Cas9 mRNA or protein at one-cell stage. Fertilized eggs were lined up against a glass slide inside a petri dish without E3 medium and injected using a thin glass needle attached to a Narishigi pico-pump injector. The needle was calibrated using a graticule (10 mm/0.1 mm graticule Ltd, Tonbridge, Kent)

guaranteeing that each pulse accurately delivered 1.4 nL into the cell. The solution filling the needle contained Cas9 mRNA and sgRNA for different genes, shown in Table 1, previously produced in the laboratory, and stored at -20°C and -80°C, respectively.

Table 1 - Summarised information about the new mutant lines created for PCD studies.

Gene	Short guide	Short guide sequence	Background
ccdc40	sg RNA1 cas9 mRNA	5- GGTAGTAGTTGAGAAGGCAG -3'	Tg(foxj1a:GFP)
ccdc39	sg RNA3 cas9 mRNA	5'- GAGGAAGATTAAAGTGAGTTTGT -3'	AB
ccdc39	sg Pol cas9 mRNA	5'- AGGAAAGACAAGGACTCAGGTGA -3'	Tg(foxj1a:GFP)
ccdc39	sg Pol cas9 protein		Tg(foxj1a:GFP)
dnah5	sg Mad cas9 mRNA	5'- CCAAGAGTTCCGCAACCTCCTCC -3'	AB
dnah5			Tg(foxj1a:GFP)
dnah11	sg 2 cas9 protein	5'- CCACGTCTAGTCATTACACCACT -3'	AB
ccno	sg RNA3 cas9 mRNA	5'- GCAGACTGTTTCCAGTTACTGGG -3'	AB

Zebrafish embryo microinjection is a routine procedure in this field, and it does not disrupt the normal development of the animals. Thus, after injection, the larvae were characterized by phenotypic observation at 3 dpf to identify the presence of curly tails or any deviations from the normal straight tails. At 5 dpf, the cilia beat frequency (CBF) of the same larvae was also assessed by high-speed video microscopy, which is described in detail in Section 3.1. To validate the aforementioned parameters and confirm the successful introduction of the desired mutations, a subset of embryos was selected for sequencing analysis. Simultaneously, the remaining embryos were maintained in an incubator set at 28°C, allowing them to develop until 5 dpf. During this period, sequencing results were awaited to determine whether these embryos would be sacrificed or integrated into the main fish facility system to grow. The following workflow was implemented:

A) Extraction of DNA

i) From a batch of embryos

A pool of 10 injected embryos at 24 or 48 hpf were placed in eppendorf tubes for DNA extraction. The maximum amount of E3 medium was removed from the eppendorf tube and 100 µL of NaOH 50 mM was added. Zebrafish were then incubated for 15 min at 95 °C. The remaining larvae were dissociated by pipetting up and down and then incubated for 5 min at 4 °C. Finally, 10 µL of Tris-HCl 10 mM (pH 9.5) was added and the mixture was centrifuged at 13 000 rpm for 10 min.

ii) From swab of ventral fin and tail fin clip

The extraction of DNA from swab of ventral fin and tail fin clip was performed in injected WT embryos that grew for at least 3 months, since that by that time it is possible to ensure the success of the extraction of DNA as well as a full recovery of the zebrafish.

In the case of swabbing, the zebrafish do not need to be anaesthetised. Zebrafish were removed from the tank with a net and placed in a petri dish. After that, the fish was trapped in the net with the ventral fin out, and the swab was obtained with a cotton tip. Once this process is complete, the zebrafish were identified and isolated in a new tank, and the tip of the swab was cut into an eppendorf tube.

For the tail fin clip, it was necessary to anaesthetize the zebrafish with tricaine (MS-222) solution at a concentration of 250 mg/L. Once the zebrafish was anesthetized, they were placed in a petri dish, and a small piece of the caudal fin was removed with a scalpel and placed on an eppendorf tube with tweezers. This procedure is delicate because the clip cannot interfere with the blood circulation of the zebrafish. If so, the zebrafish would most likely die. Similar to the previous procedure, the zebrafish were identified and isolated in a new tank once the tail fin clip was completed. Zebrafish were monitored until they were swimming again which took a few seconds.

After collecting the swab clips in eppendorf tubes, 50 µL of TE buffer was added to each sample and incubated for 10 min at 95°C. Subsequently, 8 µL of proteinase K (PK) (10 mg/mL) was added and incubated overnight (ON) at 55°C. The next day, an incubation of 10 min at 95°C was performed to inactivate PK, after which the remaining tissues were destroyed by pipetting up and down.

Sometimes, DNA was also extracted from fin clipping using NaOH and Tris-HCl, as previously described for DNA extraction from eggs.

The supernatant was stored at 4°C or immediately used as the PCR template. The DNA concentration in each sample was quantified using a Spectrophotometer Nanodrop 2000 (Thermo Scientific ND-2000 F377) before PCR. Measurement of DNA concentration revealed that the swab method for DNA extraction did not comply with the minimum concentration required to perform PCR, which was 10 ng/µL.

The PCR was performed in a thermocycler (VWR), using the specific primers for each short guide, depicted in Table 2. These primers were previously designed and optimised for each region of interest for CRISPR-Cas9 induced indels.

Table 2 - Primers flanking different gene mutation sites.

Gene Mutation	Primer Forward	Primer Reverse	PCR product size (bp)
ccdc40 sgRNA1	5'-AATCAGCTGGAAAGACTGAACC -3'	5'-CGTTGTACATTTGTTTGACTAGCAG -3'	376
ccdc39 sgPol	5'- AGATGGAAGTGCAGCGGTTG -3'	5'-CGTGACAAGTTAAAAGCGGTGATC -3	228
dnah5 sgMad	5'-CAGGTGATGTTCTGCTGGCTACTG -3'	5'- GGGGTCTGGGTCCCTTTCTAGA -3	285
dnah11 sg2	5'- TTGCCTGGGTTTCTCAGCTCC -3'	5'-CATCCCAAAACAACAGCAACGGTAA -3'	273
ccno sgRNA3	5'- AGAGGCTCGCAGTAAGCTGG -3'	5'- GCCCTGTCTCGATAGCAAACG -3'	376

After multiple attempts to optimize the PCR protocol and choose the most suitable DNA polymerase for our experiments, we established the protocol described below.

Each PCR reaction was prepared by combining 3.8 µL of Milli-Q water, 5 µL of Supreme NZYTaq II 2x Green Master Mix (nzytech MB355), 0.1 µL of each primer and 1 µL of genomic DNA adding up to a total volume of 10 µL. The PCR program was as follows: initial denaturation (96°C, 4 min), denaturation (96°C, 30 sec), annealing (60°C, 30 sec), elongation (72°C, 30 sec) and final elongation (72°C, 5 min) for 30 cycles followed by storage at 4°C.

Once the PCR was completed, the products were run on a 1% TBE-agarose gel (100 V, 30 min) to check for amplification of the desired genomic region, which is among the primers selected for each gene.

B) Heteroduplex detection

To detect heteroduplexes, PCR amplified DNA was run on a 15% Polyacrylamide Gel Electrophoresis (PAGE).

Each gel contained 6.2 mL of Milli-Q water, 1.2 mL of TBE buffer 10x (Invitrogen™ 15581044), 4.5 mL of acrylamide/bis-acrylamide 29:1 (NZYTech MB04501), 120 µL of Ammonium persulfate 10%, 9.6 µL TEMED (Bio-Rad) and allowed to polymerize between two glass plates with a 1.5 mm spacer. After 3h of electrophoresis at 150 V, the polyacrylamide gel was stained with 2 µL of GreenSafe Premium (Nzytech MB13201) diluted in 50 mL of TBE 1x buffer for 10 min, washed twice in 50 mL MilliQ-water, and visualized using Chemidoc™ XRS+ System (Bio-Rad).

Heteroduplexes arise from the annealing of two single-stranded DNA molecules originated by different sources, such as the WT and mutant alleles in heterozygous zebrafish. Because there is a change in the double-stranded conformation of DNA, its migration rate is expected to change. Generally, heteroduplexes migrate slower in PAGE than homoduplexes[119] making it a suitable method to screen heterozygous zebrafish for identifying founders. Founders are zebrafish that are expected to carry the mutations created by the CRISPR-Cas9 system and that are able to pass them on to the next generation.

Thus, when observing the polyacrylamide gel, the bands of potential heteroduplexes, as well as the respective WT bands, were cut into eppendorf tubes. For each sample, 20 µL of elution buffer was added and incubated for 3 days at 37 °C.

C) Sequencing

The DNA samples extracted from each batch of eggs or tail fins were sequenced to determine whether there were changes in the genome sequence that could correspond to the mutation created by the CRISPR-Cas9 system. The gDNA resulting from the PCR was purified (DNA clean & concentrator column Zymo research #D4003), quantified (Nanodrop™ 2000) and coupled with 3 µL of the respective

primer, forward or reverse. Then, each sample was associated with a code and sent to STABVIDA for sequencing.

By comparing the obtained sequences from the injected fish with the ones from the respective WT, it could be determined whether injected zebrafish carried a potential mutation. Once the sequences were considered promising, potential F0 zebrafish were left to grow for three months, after which it was possible to proceed with genotyping the progeny of F0 zebrafish i.e. the F1 generation.

2.2.2. Identifying founders

The term founder is only given to a certain fish when it is possible to ensure that the desired mutation is not only present in the genome of that fish but also in the genome of its progeny. To find founders, it was first necessary to cross adult potential F0 zebrafish with WT zebrafish to generate the F1 generation. The WT zebrafish were preferably *Tg(foxj1a:GFP)*, so all mutant zebrafish would have this background which marks multiciliated cells in the OP, making it easier for later microscopy analysis. When this line was not available, ABs were used as the WT zebrafish for crossings. Eggs were collected and allowed to grow for 24 h at 28 °C. When homozygous larvae were not viable after 7 dpf, the mutant lines were maintained at heterozygosity.

Once there was an F1 generation, each fish was genotyped to confirm the presence of mutations. Genotyping the F1 generation was performed as described previously for the F0 generation, by tail fin clips, performing PCR, checking for heteroduplexes on PAGE, and sequencing.

When the sequencing results were obtained and it was possible to identify alterations in the genome of the F1 generation, it was assumed that the F0 zebrafish were founders. The remaining F1 generation was allowed to grow for another three months.

2.2.3. Identifying homozygous mutants

Once the F1 zebrafish reached adulthood, they were in-crossed, and the respective eggs, already the F2 generation, were genotyped using the previously described method. Homozygous F2 zebrafish, which correspond to 25% of the population according to Mendelian laws, were expected to exhibit a curved-tail phenotype.

To confirm the exact mutation, the MEGA software was used to align the WT and expected mutant sequences to detect differences between the two. When there was a deletion, an insertion, or a substitution in the mutant genome sequence, it was possible to translate the DNA sequences to protein using the Muscle tool and determine whether the resulting protein was the same as the WT or if there was a different protein with different functions within the cilia.

Once the phenotype and genotype agreed with the expected mutations for each gene, they were used further to evaluate the recovery capacity of cilia by mRNA therapy administration. The remaining population included 50% of heterozygous zebrafish as well as 25% of WT zebrafish. This 75% was considered a control even though it was not possible to distinguish WT from heterozygous since they present the same phenotype because the mutation is recessive.

2.3. Therapy administration

The therapy employed to treat this disease utilizes the Stabilized Non-Immunogenic mRNA (SNIM®RNA) technology developed by Ethris GmbH, a German company with extensive experience in this field. Ethris GmbH has pioneered similar therapies targeting multiple PCD genes. The chemical modified RNA (cmRNA) for *CCDC40* was formulated in lipid nanoparticles (LPNs) as described in Jarzębińska et al. 2016[41]. The cmRNAs for human CCDC40 and the formulated cmRNA for human *CCDC40* were shipped in dry ice from Ethris premises to IMM, where it was kept at -80°C.

The exact formulation of this therapy remains confidential. Human mRNA, which encodes the protein affected by the *CCDC40* gene mutation, is inserted into a lipidoid nanoparticle, which is delivered to the cells by immersion of the zebrafish in a solution with nanoparticles (LNPs), stimulating topical absorption by the olfactory pit (OP). Eventhough this mode of delivery raise an extra hurdle to the carrier particles to accesing the cytoplasm by having to surpass the plasma membrane, this formulation was designed having this in consideration.

After several approaches to design the best strategy to conduct this experiment, it was decided that the more effective way to deliver the LNPs to the zebrafish, was placing the selected *CCDC40* mutants, already identified by their curly tails, in a 96 well plate, 3 larvae per well with 100 µL of medium containing 10 ng/µL of the formulated *ccdc40* cmRNA. Preliminary studies conducted in our lab suggested that

the zebrafish OP opens at 30 hpf. At this developmental time point, zebrafish larvae were incubated in a medium containing LNPs under mild agitation (50 rpm) at RT, inside a humid box to prevent evaporation. First, the larvae were incubated for 1 or 2 days (until 48 hpf or 72 hpf, respectively) and then placed in fresh medium until they reached 5 dpf (120 hpf) (Figure 7 A and B).

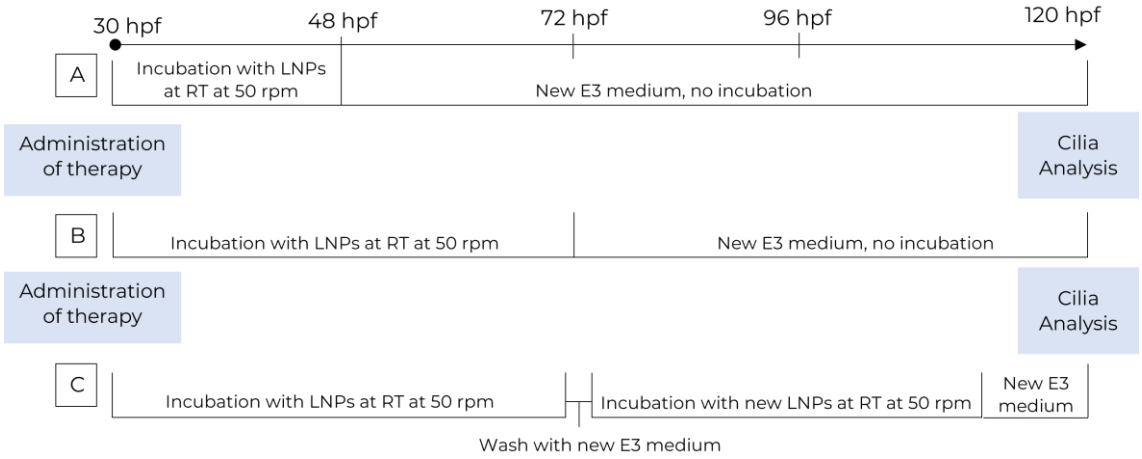

Figure 7 - Representation of 3 different strategies, A, B, and C to administer the mRNA therapy to the zebrafish mutants.

In addition, a higher concentration of mRNA (20 ng/µL) was used in this experiment to evaluate any potential impact on cilia recovery. For this, additionally to the strategies A and B applied for a lower concentration of mRNA (10 ng/µL), it was also assessed the efficacy of double administration of this therapy. For this purpose, zebrafish larvae at 30 hpf were initially incubated under the same conditions for 2 days. Subsequently, they were washed in fresh medium and subjected to an additional 2-day treatment by placing them in 100 µL of NP-containing medium (Figure 7 C). This consecutive 4 day treatment regimen allowed for the assessment of the therapy's effects. Then, the larvae were transferred to fresh medium without LNPs and allowed to develop until 5 dpf. At this stage, cilia were evaluated to determine the viability of the functional recovery.

2.4. Analysis of motile cilia function recovery

On a 5 dpf zebrafish larvae, olfactory pits can be observed as hollow cup-like structures located in the snout, as illustrated in Figure 8.

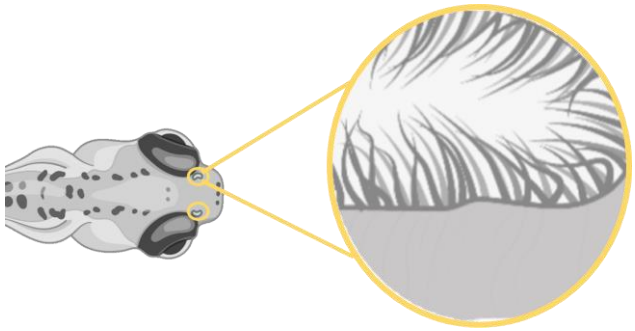

Figure 8 - Schematic representation of the olfactory pit of a 5-day post fertilization (dpf) zebrafish larva.

To evaluate the recovery of cilia functionality and measure cilia beat frequency, the treated 5 dpf larvae were anaesthetised using tricaine (MS-222) solution at a concentration of 250 mg/L. Subsequently, the larvae were carefully positioned in individual wells of a glass-bottom petri dish containing a 2% agarose mould prepared in embryonic medium. This setup facilitated the observation of cilia beating in the OP. To maintain the moisture required for the larvae, the agarose mould was filled with embryonic medium supplemented with tricaine.

The collected data underwent analysis using GraphPad Prism version 8.0.2 for Windows, developed by GraphPad Software in San Diego, California USA. Significance levels were denoted as **** for p<0,0001, *** for p<0,001 and * for p<0,05. When there was no significant difference between data, is was denoted as not significant (ns).

2.4.1. Cilia beat frequency

To characterise cilia motility and detect abnormal ciliary beat patterns in the OP of the larvae, the CBF of multiple individual cilia was analyzed. This analysis involved recording live embryos using a high-speed video microscope camera. The mounted larvae were positioned under a 40x/0.75 NA dry objective lens or a 100x/1.30 NA oil immersion objective lens on a Nikon Eclipse Ti-U inverted microscope at RT (25°C). All images were acquired with the dorsal view facing the objective lens. Bright field images were recorded with a FASTCAM MC2 camera (Photron Europe, Limited) controlled with PFV (Photron FASTCAM Viewer) software[97]. The acquired videos were produced by a collection of total consecutive 1000 frames, which corresponded to a 2 second movie at 500 frames per second (fps). CBF and quantitative analyses of motile cilia were performed using CiliarMove developed in Lopes Lab[98].

To quantify the spatial distribution of CBF, a region of interest (ROI) was selected around the studied cilia and recorded at 50 fps for 2 s (binning 1 x 1). CBF values were obtained by image filtering in ImageJ (NIH), followed by Fourier analysis in R software.

2.4.2. Rescued ciliated area

To analyze the recorded videos, Fiji's built-in selection tools were employed to manually outline the entire ciliated area in each video. The designated ROI was used to determine the fraction of ciliated areas that exhibited moving cilia in the OP.

The quantification workflow was developed using a custom-built ImageJ macro (Annex 7.1. – Ciliated area quantification). By using a Kalman filter with an acquisition noise of 0.05 and bias of 0.8, this macro filters out water flickering artefacts (Kalman Stack Filter plugin) from the image, followed by a Stack Difference with a gap of 1 to distinguish the moving particles from the stationary ones. All timepoints were Z-projected (Sum) and regions above a threshold were identified as areas with beating cilia. The fraction of ciliated area beating was calculated by dividing the thresholder area by the total ciliated area for each movie.

2.4.3. Cilia function

To evaluate the recovery of cilia function, treated larvae were immersed in a medium containing fluorescent beads, which were tracked over time. Particle Image Velocimetry (PIV) analysis and vector directionality evaluation were performed based on the movement of beads.

Using the same mounting setup for CBF measurement, 0.5 µm fluorescent beads (0.02 g/mL) (ThermoFisher F8887) were added to the wells where the larvae were positioned. The displacement of the beads was recorded using an inverted Zeiss Cell Observer SD microscope equipped with a 25x lens (LCI Plan-Neofluar Corr DIC 25x/0.8 water immersion). Images were acquired every second for 1 min. Subsequently, these videos were utilized as inputs for fluid-flow PIV analysis.

Time-lapse videos were analyzed using the PIV method with the TPIV ImageJ plugin. The parameters used were the default apart from the window's width and height (64x64 pixels). Vector coordinates, angle and length were exported as tsv files and processed using a custom Matlab script developed by Telmo Pereira (NMS Microscopy Facility). This script calculated the average length and angle over time.

3. Results

3.1. Identifying motile cilia mutants

The purpose of this study was to replicate a human PCD mutation at a corresponding location in the zebrafish genome. Previous laboratory members undertook the initial step of attempting to generate several motile cilia mutant zebrafish by microinjection using the CRISPR-Cas9 technology. Thus, my master project focused on working with adult F0-injected fish for all genes outlined in Table 1. This stage represents the most time-consuming step for mutant generation. It is not only necessary to ensure that a particular fish carries the mutation but also to guarantee that the same mutation is present in its progeny because of the challenges posed by genetic mosaicism. Therefore, the first task was to identify F0 founders by genotyping their progeny, the F1 generation (which can only present heterozygous mutants or WT larvae), to assess the presence of the desired mutations in the germline.

For this we used pools of 10 larvae with 24 hpf from the crossing of each F0 adult with a wildtype fish of the same age. After DNA extraction and PCR, the annealed PCR products were loaded and initially resolved using non-denaturing PAGE to identify heteroduplexes. The reference WT used for comparison of the PAGE results was *Tg(foxj1a:GFP)*, primarily chosen because the majority of the microinjections were performed on this genetic background. We simultaneously screened for founders for all the outlined genes, as further described in detail.

DNAH11

Concerning the *dnah11* gene, Figure 9 shows an example of PAGE analysis. Each lane shows a PCR product from the 10 pooled fish embryos. Among the seven fish screened in this example, only one pool of larvae produced favourable results, designated as founder fish number 75. The mentioned pool of fish larvae displayed discernible bands, absent in the WT reference, due to the existence of mismatches between mutated and WT sequences, indicating that some of the larvae may be heterozygous for the dnah11 gene. We observed a strong band around 273 base pairs (bp) (red box), consistent with the size of the PCR product amplified by using the designed primers. In addition, potential heteroduplexes appeared either above (300-500 bp) or slightly below (220 bp) from the reference marker (273 bp). The DNA extracted from the suspected heteroduplex (HTD) bands and the WT bands

(reference marks) were isolated for further sequence. However, DNA concentration was too low to obtain an accurate sequencing result (< 20 ng/µL). Consequently, this F0 potential founder was kept and we tried to cross it again later. Unfortunately, it would not lay more eggs, so we did not have progeny to repeat the experiment. Based on these findings, we could not pursue more F1 screening for mutations targeted to *dnah11*. Thus, we took a step back and repeated the microinjection step. Additional details regarding this matter are elaborated upon in Section 3.4.

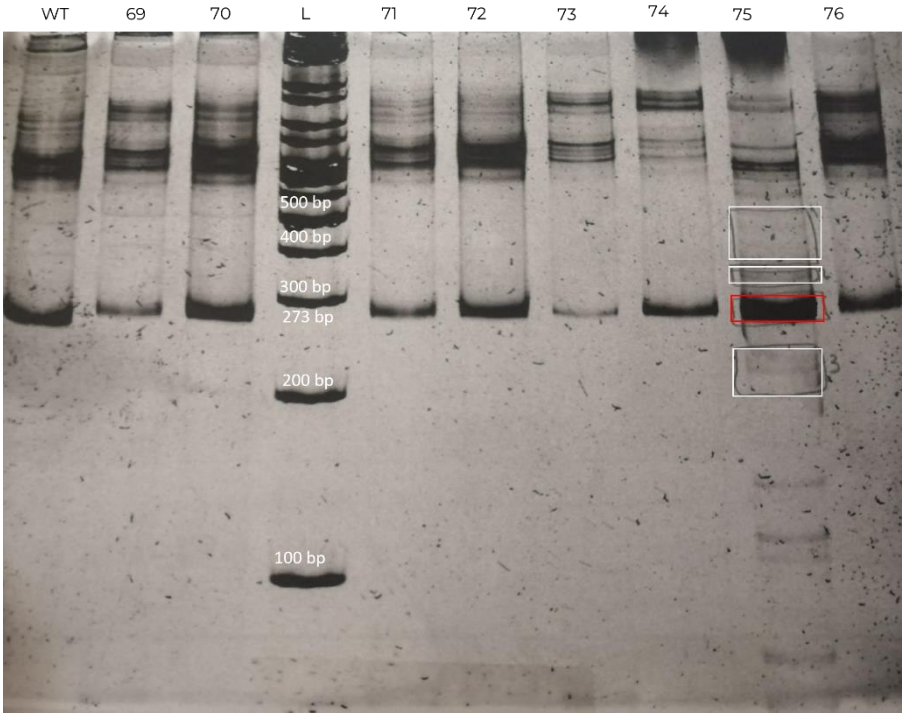

Figure 9 - Heteroduplexes detected in PAGE analysis to screen for founders of dnah11 sg2 based on a batch of larvae from F1 generation*. Each number corresponds to different potential F0 founder. The letter "L" stands for Ladder. Potential heteroduplexes are highlighted in white boxes and the reference mark correspondent to the size of the genome amplified by these primers is in the red box, approximately 273 bp.*

CCNO

Using the same approach as before we were able to identify one founder from *ccno* gene mutation (founder 6). After crossing it with a WT fish, we collected 10 embryos of the progeny to extract DNA. On a first approach, we were not able to strongly state if there was a mutation or not in this fish, so we kept the progeny while moving from CEDOC to IMM to further repeat the analysis. We extracted DNA from a new batch of embryos resulting from the cross of the founder 6 with a WT fish and, after DNA extraction and PCR, we performed sequence analysis (Figure 10).

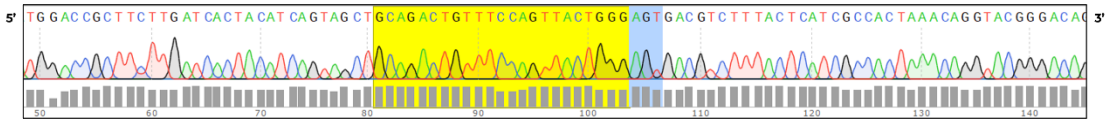

Figure 10 - Sequencing results from founder 6 ccno gene mutation. *This sequence was performed using the primer forward, therefore the PAM sequence, highlighted in blue (5'-AGT-3') is downstream the short guide sequence, highlighted in yellow, reading from 5' to 3'.*

We used the primer forward for sequencing, which means that the PAM sequence (5'-AGT-3'), highlighted in blue, is downstream of the short guide sequence (in yellow). We did not observed any particular changes in the sequence around the 100 nucleotide zone, in which the cas9 should have cut the sequence. Additionally, once set at IMM, F1 generation was already old enough to realize that we only had females on the progeny of founder 6. These two reasons led us to discard this founder and its progeny.

DNAH5

Figure 11 provides an illustrative representation of PAGE analysis for *dnah5* gene. Two specimens, identified as 7 and 8, were outined for having heteroduplexes bands, not existing in WT lane. The reference bands were, as expected approximately at 285 bp (red box), whereas the HTD bands were at 200 bp (white box).

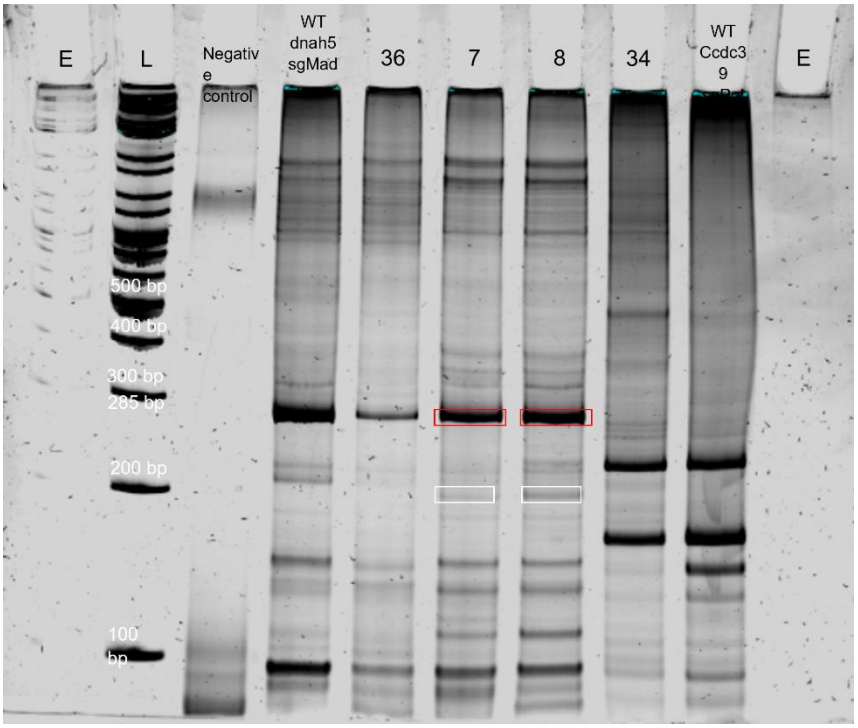

Figure 11 - Heteroduplexes detected in PAGE analysis to screen for founders of dnah5 sgMad based on a batch of larvae from F1 generation*. Each number corresponds to different potential F0 founder. The letter "L" stands for Ladder and "E" for empty well. Potential heteroduplexes are highlighted in white boxes and the reference mark correspondent to the size of the genome amplified by these primers is in the red box, approximately 285 bp.*

DNA from these bands was isolated and send to sequence. Due to the short sequence result observed (Figure 12), no conclusions could be taken. As a result, fish were kept for further screening by incross of F1 generation. F2 generation never showed any signs of abnormal tails as expected, so these founders were discarded.

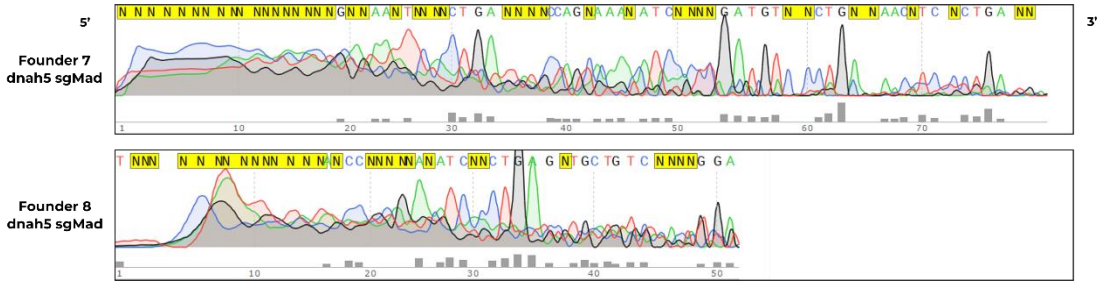

Figure 12 - Sequencing results for from founders 7 and 8 dnah5 sgMad. *The identification of the PAM and the short guide was not possible due to short sequence result.*

Further on, we were able to identify another founder, numbered 134. For this, we used the PCR product of pooled larvae to sequence. According to the sequence result shown in Figure 13, there seems to be a decrease on quality bars from position 180 which correlates with the sgRNA targeted zone. Eventhough this sequence is prone to interpretation errors, we decided to keep the fish and confirm our supposition by F1 incrossing. This is being currently done at the laboratory, as well as extraction of DNA from tail fin clips to further individual sequence analysis.

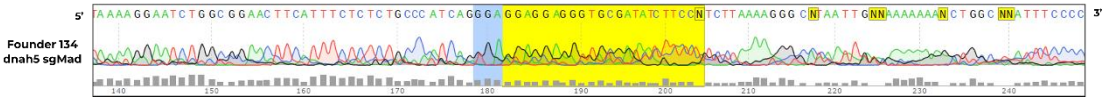

Figure 13 - Sequencing results from fish number 134 dnah5 sgMad progeny. *This sequence was performed using the primer reverse, therefore the PAM sequence, highlighted in blue (5'-GGA-3') is upstream the short guide sequence, highlighted in yellow, reading from 5' to 3'.*

Along these experiments, we also repeated the microinjection step. Additional details regarding this matter are elaborated upon in Section 3.4.

CCDC39 sgPol

Regarding the *ccdc39* gene, among the seven fish screened in the example shown on Figure 14, six pools of larvae produced favourable results, designated as founder fish number 25, 28, 29, 30, 35 and 37. The above-mentioned pools of DNA displayed discernible bands, absent in the WT reference, due to the existence of mismatches between mutated and WT sequences. We observed a strong band around 230 base pairs (bp) (red box), consistent with the size of the PCR product

amplified by using the designed primers. In addition, potential heteroduplexes appeared slightly below (200 bp) from the reference marker (230 bp).

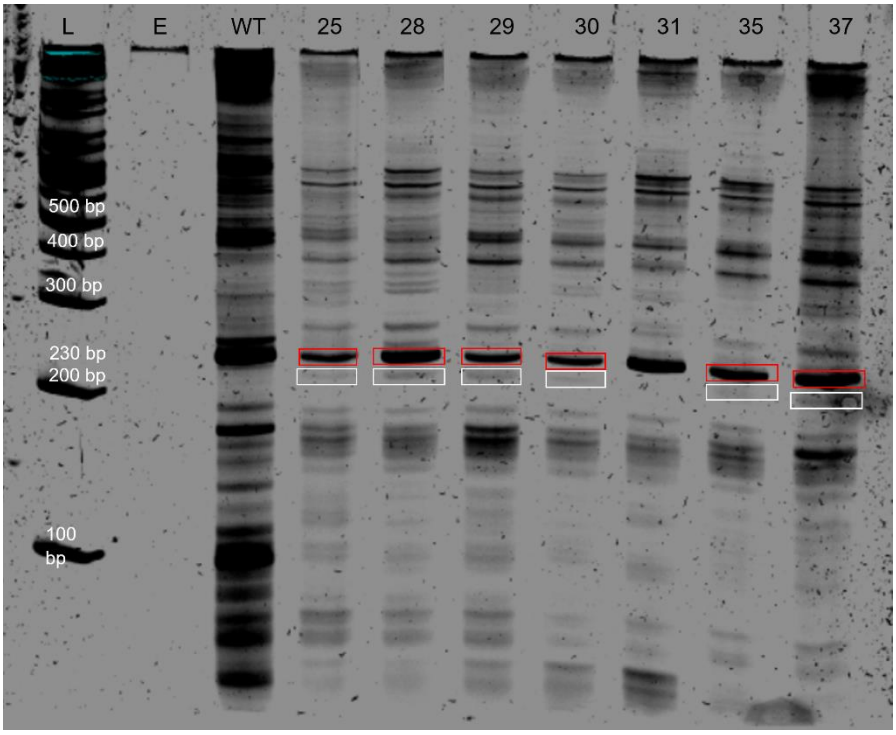

Figure 14 - Heteroduplexes detected in PAGE analysis to screen for founders of ccdc39 gene based on a batch of eggs from F1 generation. *Each number corresponds to different potential F0 founders. The letters "L" and "E" stand for Ladder and Empty wells, respectively. Potential heteroduplexes are highlighted in white boxes and the reference mark correspondent to the size of the genome amplified by these primers is in the red box (230 bp).*

The DNA extracted from the suspected heteroduplex (HTD) bands and the WT bands (reference marks) were isolated and sequenced (Figures 15 and 16). In this particular case, the primer used for sequencing was the forward, which means that the PAM sequence (5'-AAG-3'), highlighted in blue, is downstream of the short guide sequence (in yellow), reading from 5' to 3', as shown in Figure 16.

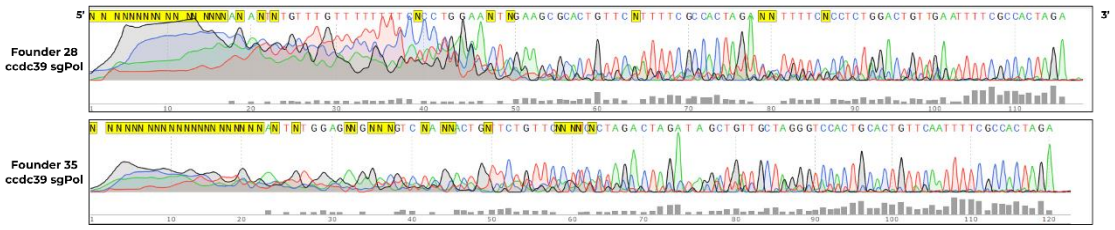

Figure 15 - Sequencing results for from founder 28 and 35 ccdc39 sgPol. *The identification of the PAM and the short guide was not possible due to short sequence result.*

DNA concentration of pools from founders 29, 30 and 37 was too low to obtain an accurate sequencing result (< 20 ng/µL). Additionally, sequencing results from bands 28, and 35 were too short to draw conclusions, since it didn't even reach the zone of the short guide (Figure 15). In a cautious manner, progenies of founders 28 and 35

were left to grow until screening could be done by incrossing the F1 generation and observing the F2 descendants. We had to discard the progeny of the founder 35 once we realized that there were only females. However, founder 28 progeny is currently being incrossed to identify homozygous mutants by detecting curly tails.

When analysing the sequencing results for founder 25, we admitted that there was an alteration of the sequence. Thus, F1 generation of founder 25 was left to grow.

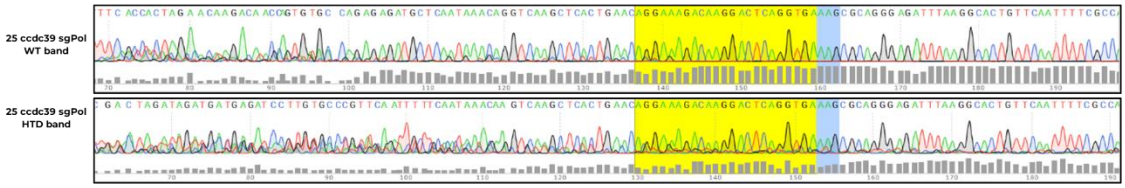

Figure 16 - Sequencing results for wildtype (WT) and from an heteroduplex (HTD) band isolated from fish number 25 ccdc39 sgPol. *The referred band (200 bp) was extracted from the gel shown in Figure 14. This sequence was performed using the primer forward, therefore the PAM sequence, highlighted in blue (5'-AAG-3') is downstream the short guide sequence, highlighted in yellow, reading from 5' to 3'.*

From this screening method based on DNA derived from a batch of ten embryos, determining the exact induced mutation is not yet possible. However, it is an effective way of assuring that the induced indels on the F0 injected fish were passed to the germline and allowed us to discard fish that did not exhibit any genomic alterations.

Heterozygous fish (F1) carrying the mutation can be identified by genotyping each of these fish by fin clipping or its progeny, F2 generation. We genotyped a batch of embryos of F2 generation and observed their phenotype at 3 dpf, where 25% of larvae must show the expected curved tail. Both approaches can be performed in parallel. Thus, we performed an in-cross of F1 fish from founder 25, and looked at their progeny. We also performed fin clipping of the F1 adult fish, when couples were unable to lay eggs.

During this step, we realized that performing PAGE analysis was not advantageous as it was very time consuming and often inconclusive; therefore, this experiment was skipped, and we decided to focus on F1 screening by sequencing.

We identified promising couples for *ccdc39* sgPol gene mutation. After in-crossing the F1 generation of *ccdc39* sgPol we did observe that some zebrafish larvae exhibited abnormal tail phenotyps (F2 generation) (Figure 18 A). However, the number of abnormal fish did not correspont to the 25% expected from Medelian laws.

Nevertheless, we proceded with analysing the F2 generation, in order to accurately identify the induced mutation produced on F0 fish. Therefore, our first task was to analyse the tail phenotype of the F2 larvae after in-crossing the F1 generation. Curled tails are the first indication of abnormal development due to motile cilia malfunction, possibly caused by genome mutations[116,117]. Nonetheless, relying solely on this information is insufficient for confirming the presence of a mutation. Therefore, we extracted DNA from larvae with both curled and straight tails and subsequently conducted sequencing after CBF measurement analysis. Figure 17 shows the experimental mounting method to acquire movies from the OP of 5 dpf larvae, mounted with a dorsal view facing the objective (Figure 17 A and B), as well as a representation of the OP image observed in the microscope (Figure 17 C).

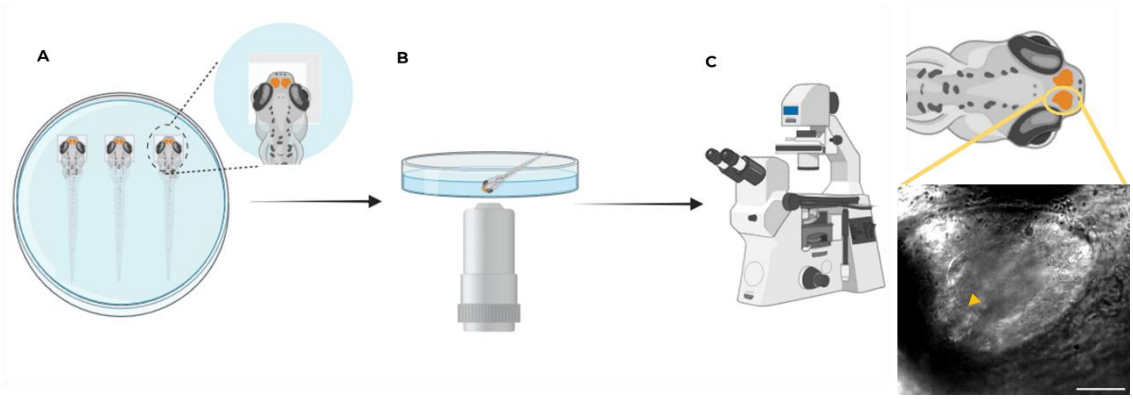

Figure 17 - Experimental mounting method for OP imaging in 5 dpf zebrafish larvae. *A) anesthetised 5 dpf larvae are placed in an agarose mould. The OP is located between the eyes on the dorsal side of the head (highlighted in orange). B) The larvae are placed with the head towards a vertical wall and the tail resting on a slope wall (side view). The slope elevates the tail, allowing the OP to rest towards the bottom of the glass dish. C) Inverted Microscopy image of the nose pit of a representative zebrafish larva. Arrowhead indicates a single cilium in a multiciliated cell. Scale Bar = 100 µm.*

To validate *ccdc39* suspected mutants we performed CBF analysis. CBF measurements of phenotypically altered *ccdc39* larvae were not distinguishable from those of WT larvae. We observed typical beating cilia in the OP with expected beating frequency values of approximately 20 Hz (Figure 18 B and C) from the frequency map and distribution graph obtained from CiliarMove. Lower CBF values (up to 5 Hz) were considered the background movement of the recorded video.

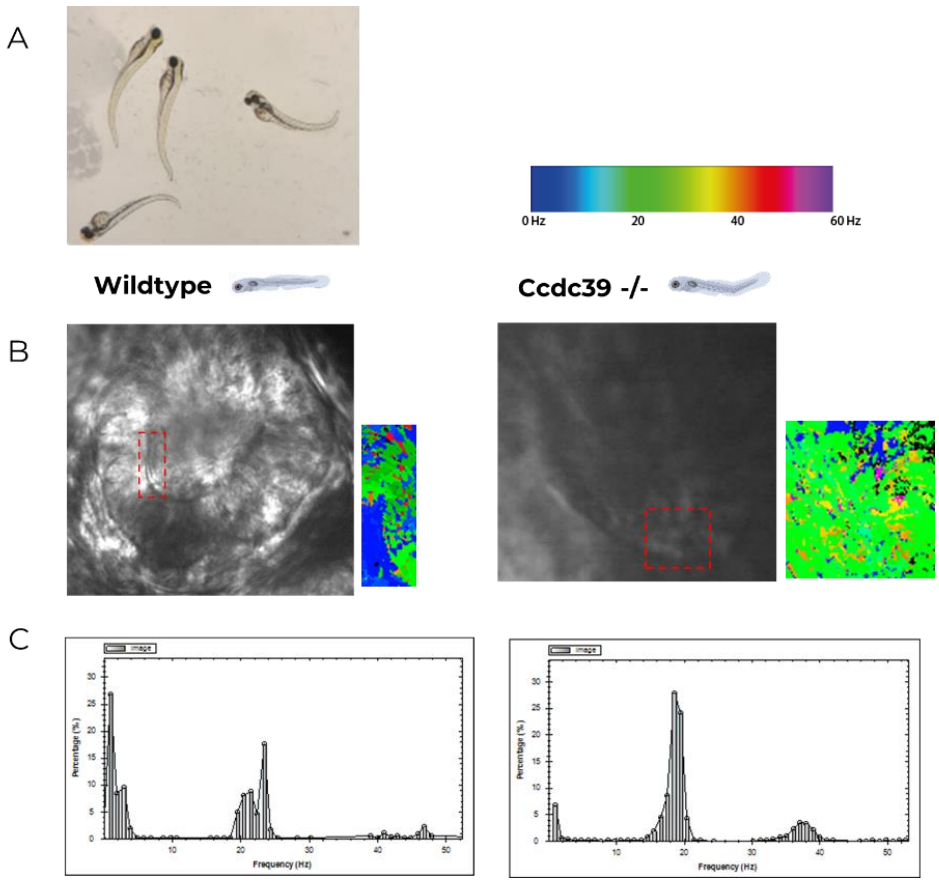

Figure 18 - Cilia movement in OP motile cilia of ccdc39 potential zebrafish mutants. *A) Curly up tailed ccdc39 possible mutant zebrafish larvae with 3 dpf. B) The images show a frame of the movies taken with an HSC in brightfield next to the heatmap obtained by processing the area of the video enclosed by the dashed line in CiliarMove. Both wildtype (left) and potential ccdc39 mutant (right) exhibit green on the correspondent ciliated area representing CBF values approximately of 20 Hz. Areas in blue are a result of absence of movement (approximately 0 Hz). C) Frequency distribution of the selected area obtained from CiliarMove. The values are in accordance with the frequency map, where the highest and more recurrent frequency is around 20 Hz. CBF values up to 5 Hz are considered background noise since they may correspond to particle movement and not cilia.*

Based on the results of CBF analysis, we thus suspected that these fish were not mutants despite the abnormal tails. This was further confirmed by sequencing, which revealed the absence of modifications in the zebrafish genome. This was confirmed through alignment of the WT sequence with the three sequences from individual larva displaying the curled-up tail phenotype (Figure 19) using the MEGA software.

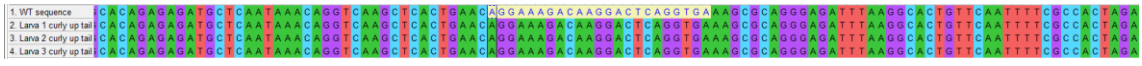

Figure 19 - Alignment of sequences from WT and individual larva with curly up tail phenotype, done in MEGA software*. Highlighted in yellow is the short guide sequence.*

Although during my project life-time, I could not identify *ccdc39* zebrafish mutants, I focused my study on the *ccdc40*$^{-/-}$, a previously identified mutant in the laboratory.

CCDC40

As previously shown in a study conducted by a colleague within the laboratory[77], a CA duplication was inserted in the genome of the *ccdc40*$^{-/-}$ line. This mutation was subsequently translated from DNA into a protein sequence using the Muscle Tool (MEGA). This analysis revealed that the insertion of two additional bases resulted in a shift in the mRNA reading frame, potentially leading to the premature occurrence of a stop codon. Consequently, the resulting protein was truncated and likely degraded.

The proper formation of the motile cilia ultrastructure strongly relies on the function of Ccdc40 protein, which serves as a crucial docking site for IDA and N-DRC components. Together with Ccdc39, these proteins establish a molecular ruler that precisely determines the attachment points for the RSs along the axoneme.

As this mutation has already been identified, our focus shifted to working with homozygous F2 zebrafish of *ccdc40* mutant line to apply LNPs formulated with CCDC40 cmRNA. Additionally, we kept on identifying more carrier couples (F1) that originates F2 curly homozygous *ccdc40* mutants.

All the work done for each gene mutation is summarized in Figure 20.

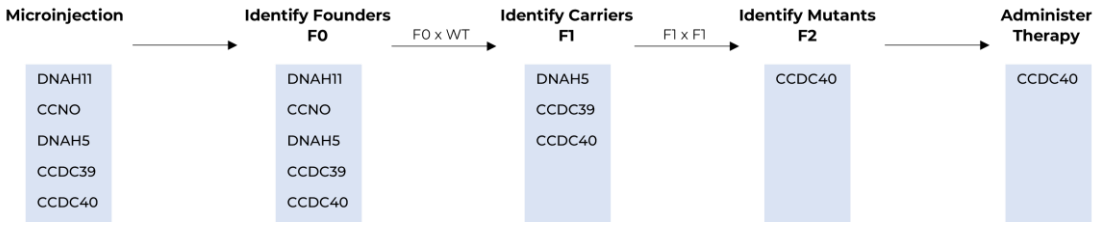

Figure 20 - Summarized workflow for each gene mutation.

3.2. Therapy administration and OP cilia movement recovery

Since PCD is a disease that interferes with the human airways, it is desirable that the mRNA therapy can be delivered by nasal inhalers to patients with PCD. Therefore, in zebrafish, the therapy was also applied topically, by immersing the larvae in a medium containing formulated lipidic nanoparticles with CCDC40 cmRNA.

Previous results from our laboratory demonstrated that the optimal starting point to deliver the therapy was approximately 30 hpf[33]. This time point corresponds to the opening of the OP to the external environment, exposing the cilia to the bathing liquid.

We tested three different exposure time-intervals, 1 day, 2 days and 4 days incubation periods with LNPs formulated with CCDC40 cmRNA at 10 ng/µL or 20 ng/µL concentration. The number of larvae filmed for each condition is summarized on Table 3.

Table 3 - Total number (n) of larvae filmed under each condition.

	Treated with mRNA at 10 ng/µL		Treated with mRNA at 20 ng/µL		Not treated	
	ccdc40$^{-/-}$	Siblings	*ccdc40*$^{-/-}$	Siblings	*ccdc40*$^{-/-}$	Siblings
1 day	10	7	10	8	10	8
2 days	9	9	15	10		
4 days	-	-	17	17		

To evaluate which incubation period and LNPs formulated with CCDC40 cmRNA concentration would promote better recovery of cilia movement, we filmed 5 dpf *ccdc40*$^{-/-}$ mutant larvae and their respective siblings subjected to the aforementioned conditions. We observed a major contrast in CBF values between *ccdc40*$^{-/-}$ larvae and their siblings either before or after treatment (Figure 21 A) (p-value<0.0001). Treated (n=51) and untreated (n=8) siblings showed the same CBF values of approximately 20 Hz. Similarly, larvae with curly tail *ccdc40*$^{-/-}$ treated (n=61) and untreated (n=10) showed CBF values of approximately 0 Hz, implying that they possessed OP motile cilia with no movement. Some *ccdc40*$^{-/-}$ treated larvae exhibited minor movements at approximately 15 Hz and higher.

We showed that some *ccdc40*$^{-/-}$ larvae still possess flickering-like movements in isolated motile cilia.

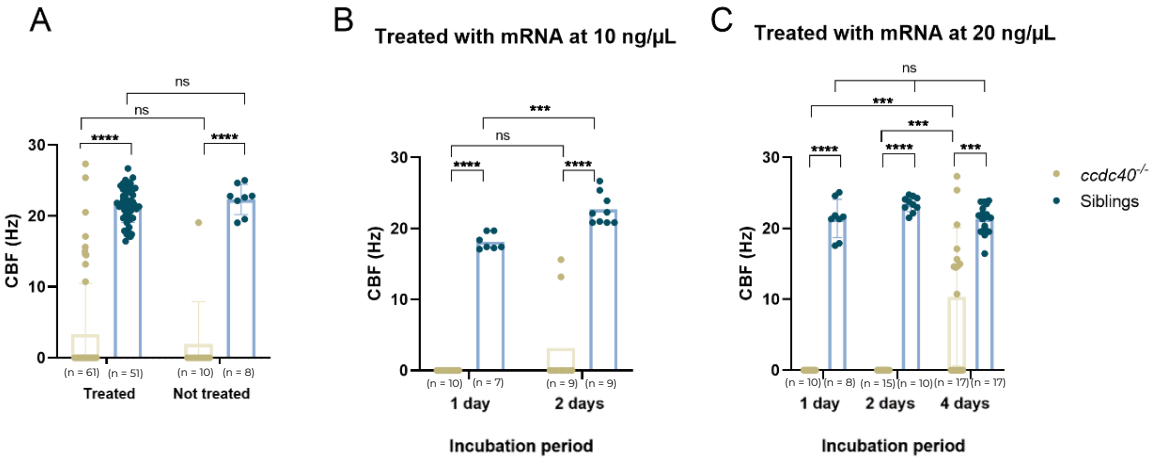

Figure 21 - Treatment of larvae with LNPs formulated CCDC40 cmRNA. *A) Cilia beat frequency (CBF) of the OP motile cilia for treated and untreated ccdc40$^{-/-}$ larvae and respective siblings. B) Incubation of ccdc40$^{-/-}$ mutants for 1 or 2 days with LNPS formulated with CCDC40 cmRNA at 10 ng/µL. C) Incubation of ccdc40$^{-/-}$ mutants for 1 , 2 or 4 days with LNPS formulated with CCDC40 cmRNA at 20 ng/µL. Unpaired t-test comparisons were conducted. Bars denote mean values, whereas individual larva are indicated by dots. *** Indicates significance with p-value< 0.001, **** indicates significance with p-value<0.0001 and ns implies not significant differences. The number of fish filmed are summarised in Table 3.*

As shown in Figure 21 B, despite a few embryos displaying cilia motility, we did not observe any significant rescue of cilia movement after treatment with LNPS formulated with CCDC40 cmRNA at 10 ng/µL, either after 1- or 2-days of incubation of *ccdc40*$^{-/-}$ larvae. Mutants with a CBF higher than zero correspond to a single cilium movement, as previously observed. This isolated event was not considered to be an effect of the therapy because it also occurs sporadicaly in untreated larvae (Figure 22).

Consequently, we aimed to test the effects of treatment with a higher cmRNA concentration by applying 20 ng/µL therapy. Nonetheless, we still did not observe any significant improvement after treating homozygous *ccdc40* mutant larvae for 1 day (n=10) or 2 days (n=15) (Figure 21 C). However, when we extended the exposure time to a 4 day incubation period, mutant *ccdc40*$^{-/-}$ larvae (n=17) showed a significant increase in CBF values. Specifically, we observed an increase from an initial value of 0 Hz before treatment to an average of 15 Hz following the 4 day incubation (Figure 21 C; p-value<0.0003) with a wide variation range until almost 30 Hz. In a total of 17 larvae filmed, almost all (n=13) showed cilia movement in the OP (Figure 22). Consequently, we admit that this increase in cilia movement is not from a single cilium, but instead because of the treatment applied, leading to the restoration of a patch of cilia in the larvae OP.

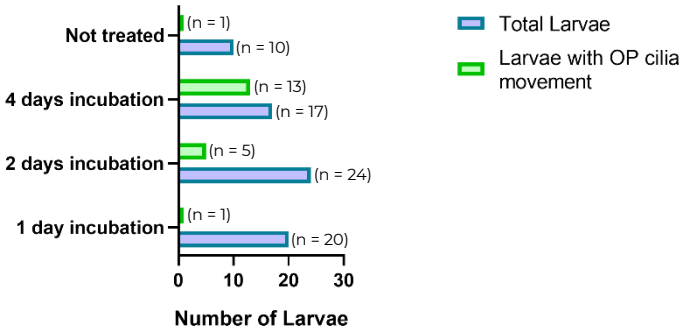

Figure 22 - Proportion of larvae with OP cilia movement. *In blue is shown the total number of ccdc40$^{-/-}$ larvae analysis whereas in green are identified those larvae that display cilia movement in the OP of zebrafish.*

However, at this point, we still could not restore the CBF values of treated *ccdc40*$^{-/-}$ to the values comparable to those of their siblings (Figure 21 C) (p-value<0.0003), the observed increase in CBF values following a 4 day incubation period is a promising step towards rescuing proper ciliary function. Moreover, as we observed beating cilia in adjacent patches in the OP, this suggests that these cilia are from a single multiciliated cell and that the administered therapy played a pivotal role in this restorative process (Supplemental videos). The videos report these rescued cases (n=13) (Supplemental videos 1, 2 and 3) as well as videos from *ccdc40*$^{-/-}$ mutants (Supplemental videos 4, 5 and 6) and their WT siblings (Supplemental videos 7, 8 and 9), which display completely different ciliary beating movements.

In summary, our findings indicate that increasing both the concentration and duration of exposure to LNPs formulated with cmRNA therapy plays a crucial role in facilitating the recovery of motile cilia function within the zebrafish larvae OP.

3.3. Additional analysis of recovery

To supplement the previous results, alongside the CBF analysis, we also wanted to assess 1) whether there was an increase of the area with movement after the administration of therapy, and 2) whether the rescued cilia in the OP could recover its function.

3.3.1. Rescued Ciliated Area

The quantification workflow of ciliated area moving within the OP included a Stack Difference with a gap of 1 to distinguish the moving particles from the stationary ones. In different consecutive images, the script recognized cilia beating because of changes in a black to white pattern in each movie. If the sum of the stacks

was high it was reflected on cilia beating. On the contrary, if the sum of stacks was low, the script would recognize only a black panel considering that cilia were not moving. To determine the proportion of ciliated area beating, we calculated it by dividing the thresholded area by the total ciliated area for each movie. This was previously done with movies acquired with a 40x objective lens which provided detailed imaging on cilia movement. We changed the objective to one of 100x to be able to observe the whole OP. Hence, a compromise had to be made in the acquisition of the movies. While we had the advantage of observing the entire OP and achieving more consistent ROIs, we did lose the finer details provided by the 40x lens when monitoring the movement of cilia.

As expected, there was a larger area with cilia movement in a *ccdc40* sibling larva OP (Figure 23 A), than in a *ccdc40*$^{-/-}$ mutant larva OP (Figure 23 B). This is depicted by more red zones in the first case than on the second, which displays no red at all. After treatment with LNPS formulated with CCDC40 cmRNA during a 4 day incubation, the script can detect a few red zones which might reflect the area of the OP which have rescued cilia (Figure 23 C).

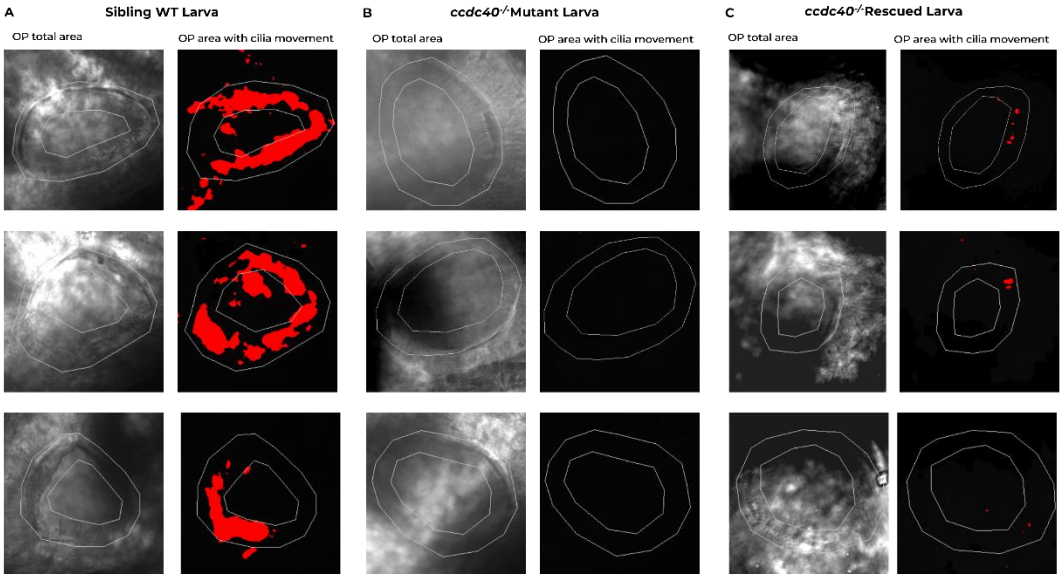

Figure 23 - Assessment of ciliated area moving in the OP of 5dpf larvae. *A), B) and C) OP total area outlined in white (left). Cilia movement (red) detected in the total OP area, after running a script on Fiji for a ccdc40 sibling larva, a mutant ccdc40*$^{-/-}$ *larva, and a ccdc40*$^{-/-}$ *larva after a 4 day incubation with LNPS formulated with CCDC40 cmRNA at 20 ng/µL (rescued). In each colum are demonstrated three examples of different larva for each condition.*

The biggest challenge in this task was to correctly position the larvae to record the videos as similar as possible concerning light, contrast, and position of the larva, to better fulfill the script parameters. As a result, even for the recorded videos of sibling larvae (n=35), where all cilia were visibly moving, the quantified area of

beating cilia is much lower than expected (p-value<0.0001) (Figure 24 A). However, since we are doing 3D live imaging, this is expected to occur. Thus, we have started to optimize the script to make it more accurate, but it is not yet fulfilling our desired parameters of sensitivity.

We measured the areas of the OP for every larva used for the last treatment experiment (n=95), with LNPs formulated with cmRNA at 20 ng/µL, since it was the only one with possible rescued OP cilia movement. The fraction of ciliated area beating is depicted, in Figure 24 B. As a result of the script employed, the ciliated areas beating quantified for the rescued *ccdc40*$^{-/-}$ do not entirely correlate with the number of larvae in which it is possible to visualize irregular cilia movement. Additionally, when cilia are potentially recovered, the pattern of movement may change. In this case, cilia do not move with more amplitude. On the contrary, cilia seem to acquire a stiffer movement with low amplitude[101]. Despite these setbacks, it is still possibly to verify an increase in the OP ciliated area beating when comparing *ccdc40*$^{-/-}$ mutants with and without treatment. This recover does not yet reach the ciliated area beating of the siblings (p-value<0.0001) (Figure 24 B), but perhaps by increasing the dose or the incubation period, we might see that occurring in future experiments.

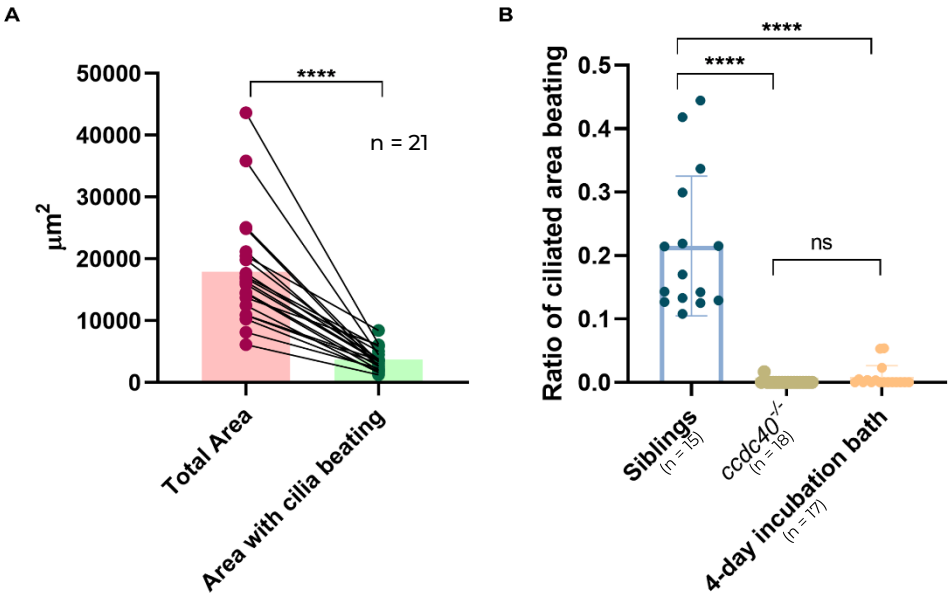

Figure 24 - Assessment of ciliated area moving in the OP of 5dpf larvae. *A) Differences at the OP ciliated area beating within the same individual of ccdc40 sibling larvae (n=21). T-test paired comparison. B) Ratio of ciliated area beating within the total OP area for the same conditions. Unpaired t-test comparisons were conducted. Bars denote mean values, whereas individual larva are indicated by dots. **** Indicates significance with p-value<0.0001 and ns implies not significant differences. The number of fish filmed are summarised in Table 3.*

3.3.2. Cilia Motility Physiology

The readout considered for the OP motile cilia function was their ability to generate a consistent water flow in and out of the OP cavity. These cilia are responsible for establishing a stereotypical flow around the nasal area. The rthytmic beating of cilia generates a quickly water flow that enters the OP, immersing the sensory receptors before being promptly expelled. This mechanism ensures constant contact between the fish's sensory cells and fresh water carrying the most recent odour molecules present in the environment[93].

To access cilia motility, 5 dpf *ccdc40* larvae were submerged in a medium containg fluorescent beads that could be monitored over time. We then conducted Particle Image Velocimetry (PIV) analysis based on the motion of these beads. In WT larvae, OP cilia draw the fluid into the medial OP regions and expel it throgh the lateral regions of the OP (Figure 25 A and B)[72,93]. On the contrary, in *ccdc40*$^{-/-}$ mutants, where cilia remain static, only Brownian motion should be detected.

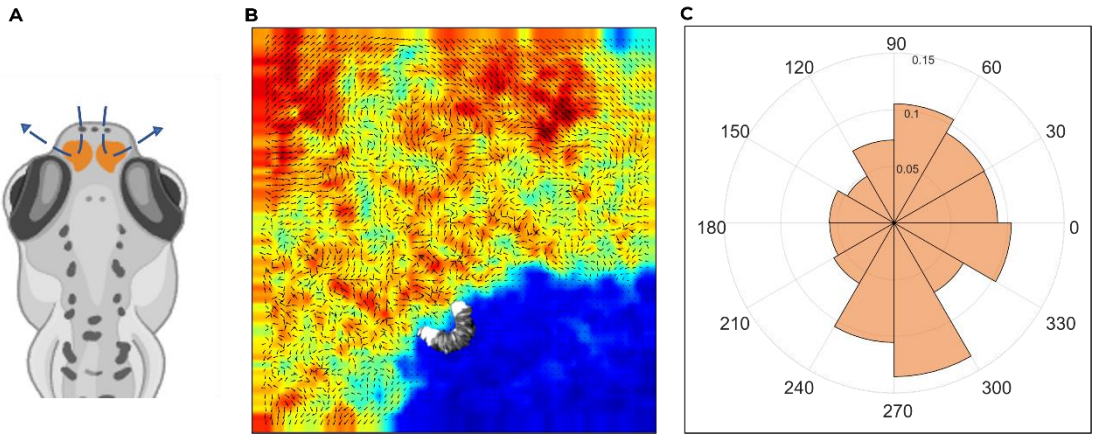

Figure 25 – Fluid flow generated by cilia movement in OP of ccdc40 wildtype zebrafish larvae. *A) Representative depiction of fluid flow direction on a wildtype larva in both OPs. This flow draws water inward from the center and pushes it outwards from the sides. B) Adding fluorescent beads to the medium evidences the fluid flow generated by the left OP cilia.. C) Rose plot resulting from the combination of the vectors from b), evidencing the intensity of the flow direction.*

For vector directionality, we depicted vectors using rose plots that displayed the strenght and orientation of the flow (Figure 25 C). Under WT conditions, the majority of vectors pointed downward due to the fluid pulling action toward the fish's nose (270°) and the lateral expulsion (240°, 300°).

It is expected that rescued *ccdc40*$^{-/-}$ larvae generate some kind of flow, even if it may be different from the one in WT controls. Nonetheless, from a translational

perspective this would be a beneficial feature, as mucociliary clearance depends on synchronization of ciliated cells.

Altogether, these two techniques are complementary experiments in our on going quest to better understand the traits of our PCD mutants. I have been actively contributing to the refinement of these methodologies, having made a considerable progress when it comes to making comparable area analysis for instance, yet it remains a dynamic work in progress, with continuous adjustments being made within the laboratory.

3.4. Characterising F0 - injected

As we were not able to identify suitable potential founders for targeted mutations in *dnah5* and *dnah11* genes, we decided to repeat the creation of mutant lines using the CRISPR-Cas9 method.

To select injected larvae for further growth, our criteria involved three key parameters: external morphological abnormalities, defects in cilia movement at the OP, and abnormal sequence analysis.

3.4.1. Tail phenotype

Our observations indicated that zebrafish embryos injected either with *dnah5* sgMad sor *dnah11* sg2 mRNA exhibited abnormal phenotypes. A significant portion of the embryos developed into larvae with malformations such as curled tails (Figure 26 B), cardiac oedema (Figure 26 C) and even cyclopia (Figure 26 D). We also identified larvae that displayed a typical phenotype (Figure 26 A).

Figure 26 - Zebrafish larvae (5 dpf) after co-injection with Cas9 protein and sgRNA for dnah5 and dnah11 gene mutations. *A) Typical looking larva B), C) and D) Zebrafish larvae with malformations, namely abnormal curly tails, cardiac oedema and cyclopia. Images acquired by Olympus MVX10 MacroView Upright Microscope. Scale Bar = 100 µm.*

When a severe deformity was observed that larva was euthanized. We only grew larvae that showed mild defects.

3.4.2. Ciliary Beat Frequency analysis

We analysed 19 individual larvae, 4 of which were injected with *dnah5* sgMad, 10 injected with *dnah11* sg2, and 5 were not injected, siblings. It is important to note that an equal number of larvae could not be filmed for each condition because of larval mortality. The average CBF was 25.39 Hz for *dnah5* sgMad injected larvae, 24.95 Hz for *dnah11* sg2 and 23.47 Hz for not injected siblings (Figure 27). A comparison of CBF values between the injected and non-injected siblings' groups revealed slightly higher CBF values for both dnah5 sgMad (p-value=0.0172) and dnah11 sg2 (p-value=0.0441). Based on these findings, we focused on a more comprehensive analysis of the injected larvae.

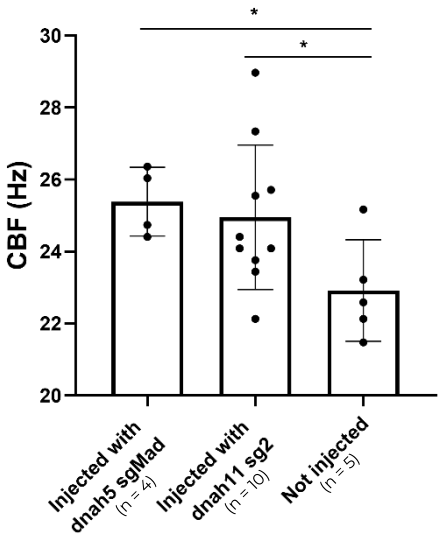

Figure 27 - Assessment of cilia beat frequency (CBF) in motile cilia of 5 dpf larvae at the OP: *dnah5 sgMad injected (n=4) , dnah11 sg2 injected (n=10), and non-injected siblings (n=5). Unpaired t-test comparisons were conducted. Bars denote mean values, whereas individual embryos are indicated by dots. * Indicates significance with p-value < 0.05.*

To confirm that using the average CBF value from both the left and right OP accurately represented each larva, we tested whether there was a difference in CBF between the two sides of the same larva. After comparing the left and right sides, we found no significant differences (n=7; p-value=0.0926) (Figure 28). This means that any observed variations were likely due to intrinsic fluctuations. Based on these results, we used the average CBF values from both sides (left and right) for each larva in all further analysis.

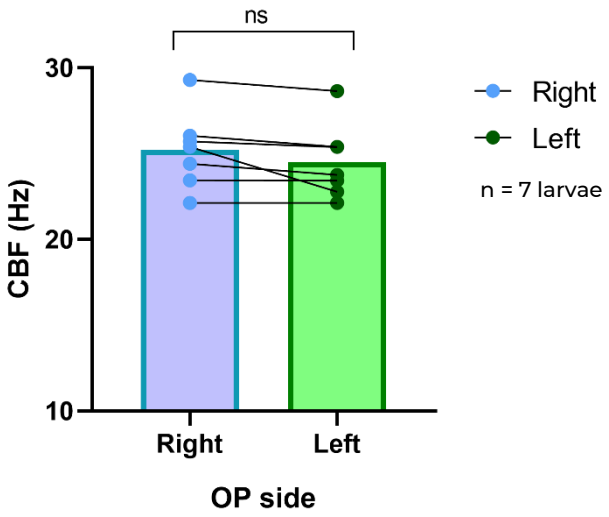

Figure 28 - Comparative analysis of CBF values between left and right OP *in 5 dpf larvae injected with dnah11 sg2. n=7. T-test paired comparison. Green colour represents the left side, blue colour represents the right side. Mean values are depicted by bars, whereas individual larvae are indicated by dots.*

3.4.2.1. Sequence analysis

Detection of mutations induced by CRISPR-Cas9 methodology can be effectively accomplished trough genome sequencing. Injections were done at one-cell stage. The injected larvae that showed severe deformities were unsuitable for our analysis because of their non-viability. Instead, our selection process involved analysing injected larvae that exhibited mild phenotypes at 5 dpf, preferably curly tails. Sequencing results were obtained from non-injected larvae (Figure 29 A) and from samples of injected larvae with *dnah5* sgMad (Figure 29 B and C).

We observed that the non-injected larvae sequences showed clear singular nucleotide peaks in the chromatogram, and it was possible to distinguish between the short guide and PAM sequences. However, sequences obtained from the injected larvae showed overlapping nucleotides in the chromatogram corresponding to the short guide and PAM region (Figure 29 B and C) and, sequences did not entirely correspond to their WT control sequence (Figure 29 A).

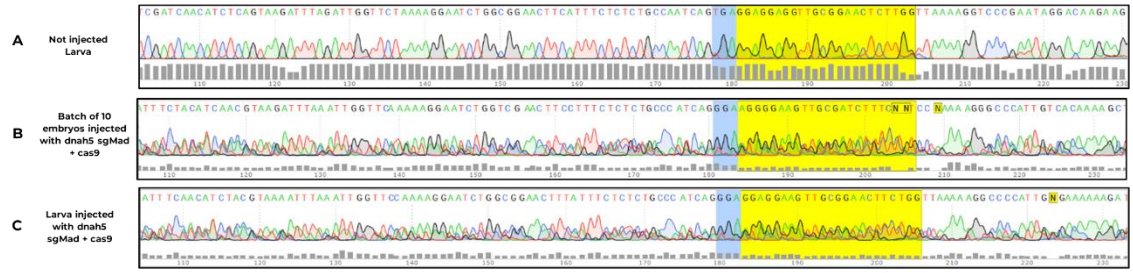

Figure 29 - Genome sequencing results after injection with dnah5 sgMad mRNA. *Sequences from A) non-injected zebrafish, B) a batch of 10 injected embryos with 24 hpf for dnah5 sgMad gene mutation, and C) one injected larva with 5 dpf. The short guide sequence is highlighted in yellow, and PAM sequence in blue.*

Furthermore, when comparing the injected larvae sequences with the control sequencing resulting from non-injected larvae, either the sequences from a batch of injected embryos or from a single defected injected larvae at 5 dpf showed low quality values associated with each nucleotide on the genome sequence, which is reflected in a disorganised and unclear sequence. Moreover, samples extracted from pools of injected embryos are expected to exhibit a less clear sequence, since they are from different individuals.

Our results suggest that the examined larvae serve as reliable indicators of the success of the injection in inducing mutations in the targeted gene region via the CRISPR-Cas9 methodology. Therefore, we transferred the remaining batch of injected fish (potential founders) to the main fish facility system to grow, and subsequently identify potential founders for the establishment of new mutant lines.

4. Discussion

During the course of my master's Project, our primary emphasis was on executing all stages involved in establishing zebrafish mutant lines. Next, we tested the eficacy of mRNA therapy to recover cilia movement in the OP of zebrafish homozyous mutant larvae.

4.1. Identifying mutants

We previously used a CRISPR-cas9 method to induce INDELs in the zebrafish, that were expected to mimic mutations on the selected PCD causing genes. To evaluate whether we had INDELs on injected generation we resorted to PAGE and sequencing analysing. This posed a significant challenge due to genetic mosaicism in animal models, resulting in a time-consuming process for identifying zebrafish mutants.

We realized that the extrapolation of results by finding heteroduplexes by PAGE analysis was very labour-intensive and it was of difficult data interpretation due to the existence of other bands that could be misinterpreted as heteroduplexes. Smaller changes in DNA mobility were therefore challenging to distinguish accurately. Furthermore, sequencing had always to be done since PAGE could not provide information about the specific nature of the mutation (deletion, insertion or substitution)[119]. As a result, PAGE analysis was overpassed, and we performed sequencing analysis instead, to make fast and more accurate decisions. In summary, our experience has shown that it is crucial to optimize primer pairs before conducting PAGE analysis in the future studies.

Nevertheless, the sequencing process was also not trivial. For each pool of fish larvae that contained heterozygous fish we were expecting an overlapping of signals in the sequencing chromatogram specifically after the PAM sequence, due to the mixture of multiple PCR fragments[2]. However, this was not always the case, or at least not immediately detected. This event led to the inexistence of a clear pattern in the sequence analysis which made us grow many larvae until adulthood to then genotype the adults by fin clipping. Thus, our work underscores the importance of dedicating time and effort to optimizing DNA extraction, purification, and PCR settings to achieve accurate sequencing results. As we showed here, not optimizing the aforementioned steps can significantly affect our conclusions when genotyping mutants. The process of identifying mutants is still ongoing in the laboratory.

We successfully overcame numerous challenges, including optimization of critical steps for mutant identification. Nevertheless, despite our efforts, we were unable to identify homozygous mutants for every targeted mutation within the selected PCD genes during the course of my project. Therefore, as a backup, we repeated the microinjection step of zebrafish embryos with Cas9 protein and mRNA for two selected short-guide genes, DNAH5 and DNAH11. To analyze the efficiency of the CRISPR-Cas9 protocol, in addition to observing body curvature, we assessed whether there would be a difference in cilia movement between the injected an uninjected siblings. We reported that injected larvae showed an increase in CBF compared to uninjected siblings. The phenotype of increased CBF has been reported previously[45]. Thus, we kept these injected larvae to grow. Previous laboratory members involved in producing other PCD model mutants did not undertake this additional step. However, we suggest that this first triage has the potential to significantly enhance the success rate of the endeavor. In addition, we also reported that there were no differences between the right and left OP from the same injected larvae at 5 dpf. This is as expected since the 2 OPs are very similar in size and shape, that only varies according to age, size of the larva and genetic variation among individuals[33]. The average CBF was rather uniform across individuals and lies between 19 and 30 Hz, as previously described by other researchers[93].

4.2. Therapy administration

Until now, there is no efficient treatment for PCD disease[31]. As a consequence, PCD patients strongly suffer from recurrent respiratory infections. To deal with this condition, patients are submitted to daily routines to help them coping with the effects of the disease, such as taking antibiotics for infection management alongside with chest physiotherapy to help clear mucus from the airways[6].

Using mRNA-based therapy has the advantage of being safer, as it does not edit the genome, and of being of rapid development, unlike gene therapy. Moreover, it allows for precise control over the design of therapeutic molecules[87]. Even though this kind of therapy is promising, it is important to note that its effects are transient and it needs to be delivered more than once, so there are still challenges to overcome like optimizing delivery methods and enhancing mRNA stability. Hence, nanoparticles encapsulating mRNA can be helpful to better monitorize and stabilize the delivery of the desired treatment[15].

Ccdc40 is an important protein to the correct assembly of IDAs. Additionally, it is also thought to be essential for recruting tubulin polyglutamilases, which are required for tubulin stabilization[56]. This event has been originally observed in *Chlamydomonas*. However, since these organisms only express the protein-coding transcript[56], it is not clear whether proteins with truncated coiled-coil domains, such as those with *ccdc40* mutations, maintain the capacity to recruit tubulin polyglutamilases. To investigate this hypothesis in the future, an antibody for polyglutamylated tubulin could be used to compare wildtype with *ccdc40*$^{-/-}$ zebrafish mutants.

The analysis of cilia beat frequency in *ccdc40*$^{-/-}$ mutant larvae revealed that OP cilia exhibit no movement (CBF = 0 Hz), which is as expected if no Ccdc40 protein is present in those cells, making IDA assembly not possible. Exceptionally, in zebrafish there can be a residual flickery movement in one or two cilium. In PCD patients, it is mostly observed a flickery movement of cilia with a reduced amplitude and stiffness[17]. This increased rigidity in cilia movement could be attributed to a remaining portion of coiled-coil domain, which allows some level of IDA assembly, that along with an intact ODA results in some residual movement[8].

The initial approach for incubation of larvae with LNPs by previous laboratory members was performed in a different manner. The protocol consisted of incubating around 20 of both selected *ccdc40*$^{-/-}$ and sibling WT larvae in a single eppendorf tube with 200 µL of medium containing 10 ng/µL of the formulated CCDC40 cmRNA for 2 days. The initial results for this delivery method showed recovery of cilia movement. Because of the risk of mortality of larvae contaminating the medium, we optimized the delivery method to avoid the death of all larvae in the eppendorf. We started to use 96 well plates with 100 µL of medium containing 10 ng/µL of the formulated CCDC40 cmRNA, each well with three larvae, for delivery with shaking. If one larva died during the incubation, we could secure the remaining wells without risking losing all larvae for the experiment. We observed some larva that displayed flickering movements at 10 ng/µL. However, this number was not statistically significant, and mutant-like flickering was discarded as a rescue by the treatment. Only when we doubled the concentration and exposure time could we observe significant rescue in CBF values using the 96 well plates. The discrepancy in CBF values observed between the two delivery methods could be explained by the methodology used. The volume of E3 medium enriched with LNPs used, the number of larvae under each experiment, and the container used, either the eppendorf or the 96 well plate,

may have caused a difference on the nanoparticle assimilation by each larvae, resulting in divergent results. Despite the aforementioned results, the well-incubation provides a lower mortality risk, enhancing experimental reliability. In conclusion, our optimization of the larval incubation method, transitioning from eppendorf tubes to 96 well plates and adjusting the concentration and exposure time of CCDC40 cmRNA led to significant improvements in rescuing ciliary movement. This emphasizes the importance of methodological considerations when comparing results.

Moreover, it is noted that after treatment with LNPS formulated with cmRNA at 20 ng/µL during a 4 day incubation period there seems to be a recovery of cilia movement in the OP of zebrafish larvae. However, CBF analysis did not match WT CBF values. It was expected that by raising the concentration of mRNA administered to the zebrafish larvae, cilia beat frequency would reach WT values, but in contrast it was spread over a wide range of values with an average of 15 Hz. An immunofluorescence analysis would be valuable in determining the distribution of human CCDC40 protein within zebrafish cilia. It is most conceavable that the protein hCCDC40 is not uniformly present along each cilium and different protein levels may be taken up by each larvae and cilia. However, to date, there is no reliable antibody available for hCCDC40, which has hindered our ability to assess its presence accurately.

So, the proof of concept for the internalization of mRNA nanoparticles, responsible for the observed increase in cilia movement as reported in this study, could be established by incorporating a small tag fused to the nanoparticles. This tagging approach would enable us to visually confirm the presence or absence of the tag within ciliated cells and subsequently correlate it with the movement pattern and CBF of motile cilia in those cells. Additionally, this strategy would shed light on whether LNPs were uniformly internalized acroos OP ciliated cels. Potential tag options include a compact fluorophore, such as tdTomato, or an HA-tag derived from the human influenza hemagglutinin (HA) molecule, with the latter requiring immunostaining to detect the HA epitope[96]. These optimizations are ongoing in the laboratory.

In an atempt to syncronize the uptake of protein, a de-ciliation of the zebrafish OP cells could be done. To do this, different approaches can be performed[88]. It can be done by submiting larvae to a pH shock[16], or we can use laser ablation to selectively remove cilia from OP multiciliated cells[71]. With these procedures, it would be

possible not only to ensure the administration of the therapy at the same time point to every larvae, assuming that the ciliogenisis is being equaly performed after disruption of cilia, but also would allow us to test if cilia motility can be rescued outside of the normal developmental time-window, for example at much later stages. Additonally, we could also test the therapy effects on OP cilia comparing cilia from ablated and non ablated neighbouring cells. Nevertheless, the de-ciliation of cells, whatever the method used, can only be performed on zebrafish larvae. When it comes to humans, it raises an ethical problem, since it would mean harming the PCD patients, with no guaranteed recovery. No ethical committee would approve such procedure.

We used a software created in the laboratory specially to evaluate the ciliary function by HVMA, CiliarMove[98]. Since it was originally generated to analyze CBF from patient nasal epithelial cells, we noticed a lack of sensitivity when it came to analysing CBF from cilia in the OP of zebrafish larvae. Nevertheless, it was a powerful tool to help us quantify cilia movement and, consequently, lead us to take major conclusions in our study. However, a better software version it is already being optimized in the laboratory. Despite the encouraging research that has documented the development of other softwares, most of these resources are not currently accessible to PCD researchers[61,90].

By the analysis of the ciliated area with cilia movement, we would like to have correlated it to the fluid flow that was generated to comprehend if the localization and magnitude of restoration of cilia on the olfactory pit would influence the direction and velocity of the fluid flow generated. However, so far we were only able to observe a recovery in cilia movement in a reduced area of the OP of zebrafish larvae. We can affirm that this restoration is possible. However, it has to be further optimized in order to obtain better results. Extrapolating these results to human PCD patients, we can hypothesize that an area inferior to 100% would make a significant difference in their daily life. It was previously shown by Ostrowski et al. 2014, that a recovery of just 20% of the cilia movement in mice respiratory epithelium improves the respiratory condition caused by PCD disease[79].

5. Conclusion

In this study, it was demonstrated by using zebrafish as an animal model for PCD disease that it is possible to recover movement of cilia present in the OP of zebrafish larvae at 5 dpf. Our observations were done in *ccdc40*$^{-/-}$ larvae after treatment with LNPS formulated with human cmRNA for the CCDC40 gene.

The most challenging task was to identify PCD zebrafish mutants, that mimic human PCD mutations, in DNAH-5, CCDC39, DNAH-11 and CCNO genes. Even though it was not possible to find homozygous mutants for each gene mutation in the time assigned for my master's project, I was able to work with a previously identified *ccdc40*$^{-/-}$ zebrafish mutant, in which I could focus on testing the mRNA-based therapy provided by Ethris GmbH.

Overall, the obtained CBF results from *ccdc40*$^{-/-}$ larvae treated with LNPS formulated with CCDC40 cmRNA at a concentration of 10 or 20 ng/µL revealed that there is no significant difference when larvae are incubated for 1 or 2 days. There is no significant increase in CBF values when comparing *ccdc40*$^{-/-}$ larvae before and after treatment under these conditions (CBF=0 Hz). However, when incubating the *ccdc40*$^{-/-}$ larvae for 4 days in medium enriched with LNPs formulated with human CCDC40 cmRNA at a concentration of 20 ng/µL, an increase in CBF values was observed in most larvae. It was observed a wide range of CBF values with an average of 15 Hz. This variety in CBF values can indicate differences in protein levels generated by each ciliated cell in each larvae. There are many steps involved in the therapy process, namely: 1) homogeneity of formulated cmRNA availability around the OP, which we optimized by shaking the incubation plates with the larvae; 2) stability of the mRNA once inside the ciliated cells; 3) success rate of translation of the mRNA into protein; 4) traffic of the replaced protein into the axoneme; 5) insertion of the ruller protein in the correct ratio. These are only some of the obvious steps we can discuss. Immunofluorescence analysis could elucidate about the level and localization of human CCDC40 protein that we can detect within the ciliated cell axonemes.

Furthermore, when analysing the OP beating ciliated area in *ccdc40*$^{-/-}$ larvae with rescued cilia compared to that in WT and mutant *ccdc40*$^{-/-}$ larvae, we observed that a reduced area of the OP was indeed moving. However, it is necessary to optimize the script that quantifies the fraction of ciliated area beating in the OP because

sometimes there were cilia moving that were not detected by the software. This may have underestimated the evaluation of rescued cilia motility.

In what regards the PCD community, this study is essential since it points out that investing in novel mRNA-based therapy strategies can recover cilia movement and function and therefore might improve patients' lives significantly. However, it is mandatory to continue exploring this field and raise awareness for this rare disease to be able to expand scientific research and complement our results with other techniques such as TEM to take a closer look at the cilia ultrastructure as well as super resolution microscopy to quantify and localize the amount of protein being held along cilia construction.

6. References

1. Alobid I, Enseñat J, Mariño-Sánchez F, De Notaris M, Centellas S, Mullol J, Bernal-Sprekelsen M. Impairment of olfaction and mucociliary clearance after expanded endonasal approach using vascularized septal flap reconstruction for skull base tumors. Neurosurgery. 2013;72(4):540–546. doi:10.1227/NEU.0b013e318282a535

2. Amorim JP, Bordeira-Carriço R, Gali-Macedo A, Perrod C, Bessa J. CRISPR-Cas9-Mediated Genomic Deletions Protocol in Zebrafish. STAR Protocols. 2020;1(3). doi:10.1016/j.xpro.2020.100208

3. Anders C, Niewoehner O, Duerst A, Jinek M. Structural basis of PAM-dependent target DNA recognition by the Cas9 endonuclease. Nature. 2014;513(7519):569–573. doi:10.1038/nature13579

4. Antony D, Becker-Heck A, Zariwala MA, Schmidts M, Onoufriadis A, Forouhan M, Wilson R, Taylor-Cox T, Dewar A, Jackson C, et al. Mutations in CCDC39 and CCDC40 are the Major Cause of Primary Ciliary Dyskinesia with Axonemal Disorganization and Absent Inner Dynein Arms. Human Mutation. 2013;34(3):462–472. doi:10.1002/humu.22261

5. Badano JL, Mitsuma N, Beales PL, Katsanis N. The ciliopathies: An emerging class of human genetic disorders. Annual Review of Genomics and Human Genetics. 2006;7:125–148. doi:10.1146/annurev.genom.7.080505.115610

6. Barbato A, Frischer T, Kuehni CE, Snijders D, Azevedo I, Baktai G, Bartoloni L, Eber E, Escribano A, Haarman E, et al. Primary ciliary dyskinesia: A consensus statement on diagnostic and treatment approaches in children. In: European Respiratory Journal. Vol. 34. 2009. p. 1264–1276. doi:10.1183/09031936.00176608

7. Bartoloni L, Blouin J-L, Pan Y, Gehrig C, Maiti AK, Scamuffa N, Rossier C, Jorissen M, Armengot M, Meeks M, et al. Mutations in the DNAH11 (axonemal heavy chain dynein type 11) gene cause one form of situs inversus totalis and most likely primary ciliary dyskinesia. www.hgmp.mrc.ac.uk

8. Becker-Heck A, Zohn IE, Okabe N, Pollock A, Lenhart KB, Sullivan-Brown J, McSheene J, Loges NT, Olbrich H, Haeffner K, et al. The coiled-coil domain containing protein CCDC40 is essential for motile cilia function and left-right axis formation. Nature Genetics. 2011;43(1):79–84. doi:10.1038/ng.727

9. Berbari NF, O'Connor AK, Haycraft CJ, Yoder BK. The Primary Cilium as a Complex Signaling Center. Current Biology. 2009;19(13). doi:10.1016/j.cub.2009.05.025

10. Blanchon S, Legendre M, Copin B, Duquesnoy P, Montantin G, Kott E, Dastot F, Jeanson L, Cachanado M, Rousseau A, et al. Delineation of CCDC39/CCDC40 mutation spectrum and associated phenotypes in primary: Ciliary dyskinesia. Journal of Medical Genetics. 2012;49(6):410–416. doi:10.1136/jmedgenet-2012-100867

11. Bolotin A, Quinquis B, Sorokin A, Dusko Ehrlich S. Clustered regularly interspaced short palindrome repeats (CRISPRs) have spacers of extrachromosomal origin. Microbiology. 2005;151(8):2551–2561. doi:10.1099/mic.0.28048-0

12. Boon M, Smits A, Cuppens H, Jaspers M, Proesmans M, Dupont LJ, Vermeulen FL, Van Daele S, Malfroot A, Godding V, et al. Primary ciliary dyskinesia: Critical evaluation of clinical symptoms and diagnosis in patients with normal and abnormal ultrastructure. Orphanet Journal of Rare Diseases. 2014;9(1). doi:10.1186/1750-1172-9-11

13. Brandsma I, Gent DC. Pathway choice in DNA double strand break repair: observations of a balancing act. 2012. http://www.genomeintegrity.com/content/3/1/9

14. Burns RG. Views and Reviews QL-, p-, and 7-Tubulins: Sequence Comparisons and Structural Constraints. 1991.

15. Byun MJ, Lim J, Kim SN, Park DH, Kim TH, Park W, Park CG. Advances in Nanoparticles for Effective Delivery of RNA Therapeutics. Biochip Journal. 2022;16(2):128–145. doi:10.1007/s13206-022-00052-5

16. Casano C, Roccheri MC, Maenza L, Migliore S, Gianguzza F. Sea urchin deciliation induces thermoresistance and activates the p38 mitogen-activated protein kinase pathway. Cell Stress and Chaperones. 2003;8(1):70–75. doi:10.1379/1466-1268(2003)8<70:SUDITA>2.0.CO;2

17. Casey JP, McGettigan PA, Healy F, Hogg C, Reynolds A, Kennedy BN, Ennis S, Slattery D, Lynch SA. Unexpected genetic heterogeneity for primary ciliary dyskinesia in the Irish Traveller population. European Journal of Human Genetics. 2015;23(2):210–217. doi:10.1038/ejhg.2014.79

18. _CCNO-mutation-as-a-cause-of-primary-ciliary-dyskinesia-A-case-reportWorld-Journal-of-Clinical-Cases.

19. Choi TY, Choi TI, Lee YR, Choe SK, Kim CH. Zebrafish as an animal model for biomedical research. Experimental and Molecular Medicine. 2021;53(3):310–317. doi:10.1038/s12276-021-00571-5

20. Coren ME, Meeks M, Morrison I, Buchdahl RM, Bush A. Primary ciliary dyskinesia: age at diagnosis and symptom history.

21. Daniels MLA, Noone PG. Genetics, diagnosis and future treatment strategies for primary ciliary dyskinesia. Expert Opinion on Orphan Drugs. 2015;3(1):31–44. doi:10.1517/21678707.2015.989212

22. Davis SD, Ferkol TW, Rosenfeld M, Lee HS, Dell SD, Sagel SD, Milla C, Zariwala MA, Pittman JE, Shapiro AJ, et al. Clinical features of childhood primary ciliary dyskinesia by genotype and ultrastructural phenotype. American Journal of Respiratory and Critical Care Medicine. 2015;191(3):316–324. doi:10.1164/rccm.201409-1672OC

23. Davy BE, Robinson ML. Congenital hydrocephalus in hy3 mice is caused by a frameshift mutation in Hydin, a large novel gene. Human Molecular Genetics. 2003;12(10):1163–1170. doi:10.1093/hmg/ddg122

24. Deltcheva E, Chylinski K, Sharma CM, Gonzales K, Chao Y, Pirzada ZA, Eckert MR, Vogel J, Charpentier E. CRISPR RNA maturation by trans-encoded small RNA and host factor RNase III. Nature. 2011;471(7340):602–607. doi:10.1038/nature09886

25. Dougherty GW, Loges NT, Klinkenbusch JA, Olbrich H, Pennekamp P, Menchen T, Raidt J, Wallmeier J, Werner C, Westermann C, et al. DNAH11 localization in the proximal region of respiratory cilia defines distinct outer dynein arm complexes. American Journal of Respiratory Cell and Molecular Biology. 2016;55(2):213–224. doi:10.1165/rcmb.2015-0353OC

26. Ferkol T. Movement. Paediatric Respiratory Reviews. 2017;24:19–20. doi:10.1016/j.prrv.2017.06.005

27. Fliegauf M, Benzing T, Omran H. When cilia go bad: Cilia defects and ciliopathies. Nature Reviews Molecular Cell Biology. 2007;8(11):880–893. doi:10.1038/nrm2278

28. Fliegauf M, Olbrich H, Horvath J, Wildhaber JH, Zariwala MA, Kennedy M, Knowles MR, Omran H. Mislocalization of DNAH5 and DNAH9 in respiratory cells from patients with primary ciliary dyskinesia. American Journal of Respiratory and Critical Care Medicine. 2005;171(12):1343–1349. doi:10.1164/rccm.200411-1583OC

29. Fliegauf M, Olbrich H, Horvath J, Wildhaber JH, Zariwala MA, Kennedy M, Knowles MR, Omran H. Mislocalization of DNAH5 and DNAH9 in respiratory cells from patients with primary ciliary dyskinesia. American Journal of Respiratory and Critical Care Medicine. 2005;171(12):1343–1349. doi:10.1164/rccm.200411-1583OC

30. Geurts MH, de Poel E, Amatngalim GD, Oka R, Meijers FM, Kruisselbrink E, van Mourik P, Berkers G, de Winter-de Groot KM, Michel S, et al. CRISPR-Based Adenine Editors Correct Nonsense Mutations in a Cystic Fibrosis Organoid Biobank. Cell Stem Cell. 2020;26(4):503-510.e7. doi:10.1016/j.stem.2020.01.019

31. Goutaki M, Papon JF, Boon M, Casaulta C, Eber E, Escudier E, Halbeisen FS, Harris A, Hogg C, Honore I, et al. Standardised clinical data from patients with primary ciliary dyskinesia: FOLLOW-PCD. ERJ Open Research. 2020;6(1). doi:10.1183/23120541.00237-2019

32. Gray KA, Yates B, Seal RL, Wright MW, Bruford EA. Genenames.org: The HGNC resources in 2015. Nucleic Acids Research. 2015;43(D1):D1079–D1085. doi:10.1093/nar/gku1071

33. Hansen A, Zeiske E. Development of the Olfactory Organ in the Zebrafish, Brachydanio rerio. 1993.

34. Henriques AR, Constant C, Descalço A, Pinto A, Moura Nunes J, Sampaio P, Lopes SS, Pereira L, Bandeira T. Primary ciliary dyskinesia due to CCNO mutations—A genotype-

phenotype correlation contribution. Pediatric Pulmonology. 2021;56(8):2776–2779. doi:10.1002/ppul.25440

35. Hom EFY, Witman GB, Harris EH, Dutcher SK, Kamiya R, Mitchell DR, Pazour GJ, Porter ME, Sale WS, Wirschell M, et al. A unified taxonomy for ciliary dyneins. Cytoskeleton. 2011;68(10):555–565. doi:10.1002/cm.20533

36. Horani A, Brody SL, Ferkol TW. Picking up speed: Advances in the genetics of primary ciliary dyskinesia. Pediatric Research. 2014;75(1–2):158–164. doi:10.1038/pr.2013.200

37. Hornef N, Olbrich H, Horvath J, Zariwala MA, Fliegauf M, Loges NT, Wildhaber J, Noone PG, Kennedy M, Antonarakis SE, et al. DNAH5 mutations are a common cause of primary ciliary dyskinesia with outer dynein arm defects. American Journal of Respiratory and Critical Care Medicine. 2006;174(2):120–126. doi:10.1164/rccm.200601-084OC

38. Howe K, Clark MD, Torroja CF, Torrance J, Berthelot C, Muffato M, Collins JE, Humphray S, McLaren K, Matthews L, et al. The zebrafish reference genome sequence and its relationship to the human genome. Nature. 2013;496(7446):498–503. doi:10.1038/nature12111

39. Ibañez-Tallon I, Heintz N, Omran H. To beat or not to beat: Roles of cilia in development and disease. Human Molecular Genetics. 2003;12(REV. ISS. 1). doi:10.1093/hmg/ddg061

40. Iliakis G, Wang H, Perrault AR, Boecker W, Rosidi B, Windhofer F, Wu W, Guan J, Terzoudi G, Panteliasc G. Mechanisms of DNA double strand break repair and chromosome aberration formation. In: Cytogenetic and Genome Research. Vol. 104. 2004. p. 14–20. doi:10.1159/000077461

41. Jarzębińska A, Pasewald T, Lambrecht J, Mykhaylyk O, Kümmerling L, Beck P, Hasenpusch G, Rudolph C, Plank C, Dohmen C. A Single Methylene Group in Oligoalkylamine-Based Cationic Polymers and Lipids Promotes Enhanced mRNA Delivery. Angewandte Chemie. 2016;128(33):9743–9747. doi:10.1002/ange.201603648

42. Jinek M, Chylinski K, Fonfara I, Hauer M, Doudna JA, Charpentier E. A Programmable Dual-RNA-Guided DNA Endonuclease in Adaptive Bacterial Immunity. http://science.sciencemag.org/

43. Kavlie RG, Kernan MJ, Eberl DF. Hearing in drosophila requires TilB, a conserved protein associated with ciliary motility. Genetics. 2010;185(1):177–188. doi:10.1534/genetics.110.114009

44. King SM. Axonemal dynein arms. Cold Spring Harbor Perspectives in Biology. 2016;8(11). doi:10.1101/cshperspect.a028100

45. Knowles MR, Leigh MW, Carson JL, Davis SD, Dell SD, Ferkol TW, Olivier KN, Sagel SD, Rosenfeld M, Burns KA, et al. Mutations of DNAH11 in patients with primary ciliary dyskinesia with normal ciliary ultrastructure. Thorax. 2012;67(5):433–441. doi:10.1136/thoraxjnl-2011-200301

46. Knowles MR, Zariwala M, Leigh M. Primary Ciliary Dyskinesia. Clinics in Chest Medicine. 2016;37(3):449–461. doi:10.1016/j.ccm.2016.04.008

47. Kobayashi D, Takeda H. Ciliary motility: The components and cytoplasmic preassembly mechanisms of the axonemal dyneins. Differentiation. 2012;83(2). doi:10.1016/j.diff.2011.11.009

48. Kozminski KG, Johnson KA, Forscher P, Rosenbaum JL. A motility in the eukaryotic flagellum unrelated to flagellar beating (Chlamydomonas/ntrelular movement/ultrastcture). 1993.

49. Kubo T, Yagi T, Kamiya R. Tubulin polyglutamylation regulates flagellar motility by controlling a specific inner-arm dynein that interacts with the dynein regulatory complex. Cytoskeleton. 2012;69(12):1059–1068. doi:10.1002/cm.21075

50. Kuehni CE, Frischer T, Strippoli MPF, Maurer E, Bush A, Nielsen KG, Escribano A, Lucase JSA, Yiallouros P, Omran H, et al. Factors influencing age at diagnosis of primary ciliary dyskinesia in European children. European Respiratory Journal. 2010;36(6):1248–1258. doi:10.1183/09031936.00001010

51. Kuehni CE, Lucas JS. Diagnosis of primary ciliary dyskinesia: Summary of the ERS task force report. Breathe. 2017;13(3):166–178. doi:10.1183/20734735.008517

52. Lane N. The unseen World: Reflections on Leeuwenhoek (1677) 'Concerning little animals.' Philosophical Transactions of the Royal Society B: Biological Sciences. 2015;370(1666). doi:10.1098/rstb.2014.0344

53. leewenhoeck. vanleewenhoeck1677.

54. Leigh MW, Ferkol TW, Davis SD, Lee HS, Rosenfeld M, Dell SD, Sagel SD, Milla C, Olivier KN, Sullivan KM, et al. Clinical features and associated likelihood of primary ciliary dyskinesia in children and adolescents. Annals of the American Thoracic Society. 2016;13(8):1305–1313. doi:10.1513/AnnalsATS.201511-748OC

55. Lieber MR. The mechanism of double-strand DNA break repair by the nonhomologous DNA end-joining pathway. Annual Review of Biochemistry. 2010;79:181–211. doi:10.1146/annurev.biochem.052308.093131

56. Lin H, Zhang Z, Guo S, Chen F, Kessler JM, Wang YM, Dutcher SK. A NIMA-Related Kinase Suppresses the Flagellar Instability Associated with the Loss of Multiple Axonemal Structures. PLoS Genetics. 2015;11(9). doi:10.1371/journal.pgen.1005508

57. Lin J, Nicastro D. Asymmetric distribution and spatial switching of dynein activity generates ciliary motility. Science. 2018;360(6387). doi:10.1126/science.aar1968

58. Lin J, Tritschler D, Song K, Barber CF, Cobb JS, Porter ME, Nicastro D. Building blocks of the nexin-dynein regulatory complex in chlamydomonas flagella. Journal of Biological Chemistry. 2011;286(33):29175–29191. doi:10.1074/jbc.M111.241760

59. Liu Y, Liang F, Dong Z, Li S, Ye J, Qin W. Genome editing in zebrafish by ScCas9 recognizing NNG PAM. Cells. 2021;10(8). doi:10.3390/cells10082099

60. Loges NT, Antony D, Maver A, Deardorff MA, Güleç EY, Gezdirici A, Nöthe-Menchen T, Höben IM, Jelten L, Frank D, et al. Recessive DNAH9 Loss-of-Function Mutations Cause Laterality Defects and Subtle Respiratory Ciliary-Beating Defects. American Journal of Human Genetics. 2018;103(6):995–1008. doi:10.1016/j.ajhg.2018.10.020

61. Lu C, Marx M, Zahid M, Lo CW, Chennubhotla C, Quinn SP. Stacked Neural Networks for end-to-end ciliary motion analysis. 2018 Mar 20. http://arxiv.org/abs/1803.07534

62. Lucas JS, Barbato A, Collins SA, Goutaki M, Behan L, Caudri D, Dell S, Eber E, Escudier E, Hirst RA, et al. European Respiratory Society guidelines for the diagnosis of primary ciliary dyskinesia. European Respiratory Journal. 2017;49(1). doi:10.1183/13993003.01090-2016

63. Makarova KS, Haft DH, Barrangou R, Brouns SJJ, Charpentier E, Horvath P, Moineau S, Mojica FJM, Wolf YI, Yakunin AF, et al. Evolution and classification of the CRISPR-Cas systems. Nature Reviews Microbiology. 2011;9(6):467–477. doi:10.1038/nrmicro2577

64. Merveille AC, Davis EE, Becker-Heck A, Legendre M, Amirav I, Bataille G, Belmont J, Beydon N, Billen F, Clément A, et al. CCDC39 is required for assembly of inner dynein arms and the dynein regulatory complex and for normal ciliary motility in humans and dogs. Nature Genetics. 2011;43(1):72–78. doi:10.1038/ng.726

65. Miki H, Setou M, Kaneshiro K, Hirokawa N. All kinesin superfamily protein, KIF, genes in mouse and human. www.pnas.org

66. Mitchell DR. The Evolution of Eukaryotic Cilia and Flagella as Motile and Sensory Organelles.

67. Mitchison HM, Valente EM. Motile and non-motile cilia in human pathology: from function to phenotypes. Journal of Pathology. 2017;241(2):294–309. doi:10.1002/path.4843

68. Mojica FJM, Díez-Villaseñor C, García-Martínez J, Soria E. Intervening sequences of regularly spaced prokaryotic repeats derive from foreign genetic elements. Journal of Molecular Evolution. 2005;60(2):174–182. doi:10.1007/s00239-004-0046-3

69. Mullowney T, Manson D, Kim R, Stephens D, Shah V, Dell S. Primary ciliary dyskinesia and neonatal respiratory distress. Pediatrics. 2014;134(6):1160–1166. doi:10.1542/peds.2014-0808

70. N H. Kinesin and dynein superfamily. S. Carpenter; 1998. www.sciencemag.org

71. Nedved BT, Freckelton ML, Hadfield MG. Laser ablation of the apical sensory organ of Hydroides elegans (Polychaeta) does not inhibit detection of metamorphic cues. Journal of Experimental Biology. 2021;224(20). doi:10.1242/jeb.242300

72. Neuhauss SCF. Olfaction: How Fish Catch a Whiff. Current Biology. 2017;27(2):R57–R58. doi:10.1016/j.cub.2016.12.007

73. Nicastro D, Schwartz C, Pierson J, Gaudette R, Porter ME, Mcintosh JR. The Molecular Architecture of Axonemes Revealed by Cryoelectron Tomography. www.sciencemag.org

74. Noone PG, Leigh MW, Sannuti A, Minnix SL, Carson JL, Hazucha M, Zariwala MA, Knowles MR. Primary Ciliary Dyskinesia. American Journal of Respiratory and Critical Care Medicine. 2004;169(4):459–467. https://www.atsjournals.org/doi/10.1164/rccm.200303-365OC. doi:10.1164/rccm.200303-365OC

75. Oda T, Yanagisawa H, Kamiya R, Kikkawa M. A molecular ruler determines the repeat length in eukaryotic cilia and flagella. Science. 2014;346(6211):857–860. doi:10.1126/science.1260214

76. Olbrich H, Häffner K, Kispert A, Völkel A, Volz A, Sasmaz G, Reinhardt R, Hennig S, Lehrach H, Konietzko N, et al. Mutations in DNAH5 cause primary ciliary dyskinesia and randomization of left-right asymmetry. Nature Genetics. 2002;30(2):143–144. doi:10.1038/ng817

77. Oliveira Almeida Rasteiro M, Susana Lopes Professora Doutora Rita Zilhão D. UNIVERSIDADE DE LISBOA FACULDADE DE CIÊNCIAS DEPARTAMENTO DE BIOLOGIA VEGETAL Creation of a Danio rerio mutant using CRISPR-Cas9 as a model system to study Primary Ciliary Dyskinesia (PCD). 2017.

78. Omran H, Kobayashi D, Olbrich H, Tsukahara T, Loges NT, Hagiwara H, Zhang Q, Leblond G, O'Toole E, Hara C, et al. Ktu/PF13 is required for cytoplasmic pre-assembly of axonemal dyneins. Nature. 2008;456(7222):611–616. doi:10.1038/nature07471

79. Ostrowski LE, Yin W, Patel M, Sechelski J, Rogers T, Burns K, Grubb BR, Olsen JC. Restoring ciliary function to differentiated primary ciliary dyskinesia cells with a lentiviral vector. Gene Therapy. 2014;21(3):253–261. doi:10.1038/gt.2013.79

80. Papon JF, Coste A, Roudot-Thoraval F, Boucherat M, Roger G, Tamalet A, Vojtek AM, Amselem S, Escudier E. A 20-year experience of electron microscopy in the diagnosis of primary ciliary dyskinesia. European Respiratory Journal. 2010;35(5):1057–1063. doi:10.1183/09031936.00046209

81. Pazour GJ, Agrin N, Leszyk J, Witman GB. Proteomic analysis of a eukaryotic cilium. Journal of Cell Biology. 2005;170(1):103–113. doi:10.1083/jcb.200504008

82. Peeters H, Devriendt K. Human laterality disorders. European Journal of Medical Genetics. 2006;49(5):349–362. doi:10.1016/j.ejmg.2005.12.003

83. Peng B, Gao Y hua, Xie J qi, He X wen, Wang C cong, Xu J fu, Zhang G jun. Clinical and genetic spectrum of primary ciliary dyskinesia in Chinese patients: a systematic review. Orphanet Journal of Rare Diseases. 2022;17(1). doi:10.1186/s13023-022-02427-1

84. Pintado P, Sampaio P, Tavares B, Montenegro-Johnson TD, Smith DJ, Lopes SS. Dynamics of cilia length in left–right development. Royal Society Open Science. 2017;4(3). doi:10.1098/rsos.161102

85. Pinto AL, Rasteiro M, Bota C, Pestana S, Sampaio P, Hogg C, Burgoyne T, Lopes SS. Zebrafish motile cilia as a model for primary ciliary dyskinesia. International Journal of Molecular Sciences. 2021;22(16). doi:10.3390/ijms22168361

86. Porter ME, Sale WS. Mini-Review The 9 2 Axoneme Anchors Multiple Inner Arm Dyneins and a Network of Kinases and Phosphatases that Control Motility. 2000. http://www.jcb.org/cgi/content/full/151/5/F37

87. Qin S, Tang X, Chen Y, Chen K, Fan N, Xiao W, Zheng Q, Li G, Teng Y, Wu M, et al. mRNA-based therapeutics: powerful and versatile tools to combat diseases. Signal Transduction and Targeted Therapy. 2022;7(1). doi:10.1038/s41392-022-01007-w

88. Quarmby LM. Cellular Deflagellation. 2004.

89. Quarmby LM, Parker JDK. Cilia and the cell cycle? Journal of Cell Biology. 2005;169(5):707–710. doi:10.1083/jcb.200503053

90. Quinn SP, Zahid MJ, Durkin JR, Francis RJ, Lo CW, Chennubhotla SC. Automated identification of abnormal respiratory ciliary motion in nasal biopsies. Science Translational Medicine. 2015;7(299). doi:10.1126/scitranslmed.aaa1233

91. Rafael P, De M, Sampaio A. UNCOUPLING HEART AND LIVER LATERALITY EVENTS DURING EMBRYOGENESIS Tese para obtenção do grau de Doutor em Mecanismos de Doença e Medicina Regenerativa Doutoramento em associação entre.

92. Raidt J, Wallmeier J, Hjeij R, Onnebrink JG, Pennekamp P, Loges NT, Olbrich H, Häffner K, Dougherty GW, Omran H, et al. Ciliary beat pattern and frequency in genetic variants of primary ciliary dyskinesia. European Respiratory Journal. 2014;44(6):1579–1588. doi:10.1183/09031936.00052014

93. Reiten I, Uslu FE, Fore S, Pelgrims R, Ringers C, Diaz Verdugo C, Hoffman M, Lal P, Kawakami K, Pekkan K, et al. Motile-Cilia-Mediated Flow Improves Sensitivity and Temporal Resolution of Olfactory Computations. Current Biology. 2017;27(2):166–174. doi:10.1016/j.cub.2016.11.036

94. Roossien DH, Miller KE, Gallo G. Ciliobrevins as tools for studying dynein motor function. Frontiers in Cellular Neuroscience. 2015;9(JULY). doi:10.3389/fncel.2015.00252

95. Rosenbaum JL, Witman GB. Intraflagellar transport. Nature Reviews Molecular Cell Biology. 2002;3(11):813–825. doi:10.1038/nrm952

96. Rui Y, Wilson DR, Tzeng SY, Yamagata HM, Sudhakar D, Conge M, Berlinicke CA, Zack DJ, Tuesca A, Green JJ. H E A L T H A N D M E D I C I N E High-throughput and high-content bioassay enables tuning of polyester nanoparticles for cellular uptake, endosomal escape, and systemic in vivo delivery of mRNA. 2022. https://www.science.org

97. Sampaio P, Ferreira RR, Guerrero A, Pintado P, Tavares B, Amaro J, Smith AA, Montenegro-Johnson T, Smith DJ, Lopes SS. Left-right organizer flow dynamics: How much cilia activity reliably yields laterality? Developmental Cell. 2014;29(6):716–728. doi:10.1016/j.devcel.2014.04.030

98. Sampaio P, da Silva MF, Vale I, Roxo-Rosa M, Pinto A, Constant C, Pereira L, Quintão CM, Lopes SS. Ciliarmove: New software for evaluating ciliary beat frequency helps find novel mutations by a portuguese multidisciplinary team on primary ciliary dyskinesia. ERJ Open Research. 2021;7(1):1–12. doi:10.1183/23120541.00792-2020

99. Satir P. CILIA: Before and after. Cilia. 2017;6(1). doi:10.1186/s13630-017-0046-8

100. Satir P. STUDIES ON CILIA The Fixation of the Metaehronal Wave.

101. Schwabe GC, Hoffmann K, Loges NT, Birker D, Rossier C, De Santi MM, Olbrich H, Fliegauf M, Failly M, Liebers U, et al. Primary ciliary dyskinesia associated with normal axoneme ultrastructure is caused by DNAH11 mutations. Human Mutation. 2008;29(2):289–298. doi:10.1002/humu.20656

102. Shapiro AJ, Davis SD, Ferkol T, Dell SD, Rosenfeld M, Olivier KN, Sagel SD, Milla C, Zariwala MA, Wolf W, et al. Laterality defects other than situs inversus totalis in primary ciliary dyskinesia: Insights into situs ambiguus and heterotaxy. Chest. 2014;146(5):1176–1186. doi:10.1378/chest.13-1704

103. Shapiro AJ, Davis SD, Polineni D, Manion M, Rosenfeld M, Dell SD, Chilvers MA, Ferkol TW, Zariwala MA, Sagel SD, et al. Diagnosis of primary ciliary dyskinesia: An official American thoracic society clinical practice guideline. American Journal of Respiratory and Critical Care Medicine. 2018;197(12):e24–e39. doi:10.1164/rccm.201805-0819ST

104. Shapiro AJ, Zariwala MA, Ferkol T, Davis SD, Sagel SD, Dell SD, Rosenfeld M, Olivier KN, Milla C, Daniel SJ, et al. Diagnosis, monitoring, and treatment of primary ciliary dyskinesia: PCD foundation consensus recommendations based on state of the art review. Pediatric Pulmonology. 2016;51(2):115–132. doi:10.1002/ppul.23304

105. Sleigh MA, Blake JR, Llron N. State of Art The Propulsion of Mucus by Cilia 1-3.

106. Sudipta Pandit, Sabyasachi Choudhury, Anirban Das, Sumitra Basuthakur, Sibes Kumar Das. A rare case of Kartagener's syndrome. Journal of Natural Science, Biology and Medicine. 2014 Jun:175–177.

107. Sui W, Hou X, Che W, Ou M, Sun G, Huang S, Liu F, Chen P, Wei X, Dai Y. CCDC40 mutation as a cause of primary ciliary dyskinesia: a case report and review of literature. Clinical Respiratory Journal. 2016;10(5):614–621. doi:10.1111/crj.12268

108. Vincensini L, Blisnick T, Bastin P. 1001 model organisms to study cilia and flagella. Biology of the Cell. 2011;103(3):109–130. doi:10.1042/bc20100104

109. Vuolo L, Stevenson NL, Mukhopadhyay AG, Roberts AJ, Stephens DJ. Cytoplasmic dynein-2 at a glance. Journal of Cell Science. 2020;133(6). doi:10.1242/jcs.240614

110. Wallmeier J, Al-Mutairi DA, Chen CT, Loges NT, Pennekamp P, Menchen T, Ma L, Shamseldin HE, Olbrich H, Dougherty GW, et al. Mutations in CCNO result in congenital mucociliary clearance disorder with reduced generation of multiple motile cilia. Nature Genetics. 2014;46(6):646–651. doi:10.1038/ng.2961

111. Wallmeier J, Nielsen KG, Kuehni CE, Lucas JS, Leigh MW, Zariwala MA, Omran H. Motile ciliopathies. Nature Reviews Disease Primers. 2020;6(1). doi:10.1038/s41572-020-0209-6

112. Walton RT, Christie KA, Whittaker MN, Kleinstiver BP. Unconstrained genome targeting with near-PAMless engineered CRISPR-Cas9 variants. Science. 2020;368(6488):290–296. doi:10.1126/science.aba8853

113. Werner-Peterson R, Sloboda RD. Methylation of structural components of the axoneme occurs during flagellar disassembly. Biochemistry. 2013;52(47):8501–8509. doi:10.1021/bi4011623

114. Wheway G, Nazlamova L, Hancock JT. Signaling through the primary cilium. Frontiers in Cell and Developmental Biology. 2018;6(FEB). doi:10.3389/fcell.2018.00008

115. Yan L, Zheng YF. Cilia and their role in neural tube development and defects. Reproductive and Developmental Medicine. 2022;6(2):67–78. doi:10.1097/RD9.0000000000000014

116. Zhang X, Jia S, Chen Z, Chong YL, Xie H, Feng D, Wu X, Song DZ, Roy S, Zhao C. Cilia-driven cerebrospinal fluid flow directs expression of urotensin neuropeptides to straighten the vertebrate body axis. Nature Genetics. 2018;50(12):1666–1673. doi:10.1038/s41588-018-0260-3

117. Zhao C, Malicki J. Genetic defects of pronephric cilia in zebrafish. Mechanisms of Development. 2007;124(7–8):605–616. doi:10.1016/j.mod.2007.04.004

118. Zhu X, Liu Y, Yang P. Radial spokes—a snapshot of the motility regulation, assembly, and evolution of cilia and flagella. Cold Spring Harbor Perspectives in Biology. 2017;9(5). doi:10.1101/cshperspect.a028126

119. Zhu X, Xu Y, Yu S, Lu L, Ding M, Cheng J, Song G, Gao X, Yao L, Fan D, et al. An efficient genotyping method for genome-modified animals and human cells generated with CRISPR/Cas9 system. Scientific Reports. 2014;4. doi:10.1038/srep06420

7. Annexes

7.1. Ciliated area quantification

```
// Init
fdir  = File.directory;
//fdir = "D:/Users/ASUS/Desktop/TESE/RESULTADOS"
run("Set Measurements...", "area mean integrated area_fraction limit display redirect=None decimal=3");
roiManager("reset");
run("Clear Results");
title = getTitle();
thresh = 2580;

// macro
//run("Kalman Stack Filter", "acquisition_noise=0.05 bias=0.80");
run("Stack Difference", "gap=1");
run("Slice Remover", "first=1 last=10 increment=1");
run("Slice Remover", "first=980 last="+nSlices+" increment=1");
run("Median...", "radius=2 stack");
run("Z Project...", "projection=[Sum Slices]");
selectWindow(title);
//waitForUser;
roiManager("Add");
selectWindow("SUM_Difference Image");
rename("STD_" + title);
roiManager("Select", 0);
run("Measure");
//setThreshold(thresh, 1000000000000000000000000000000.0000);
run("Threshold...");
waitForUser;
run("Measure");



//cleanup
```

```
roiManager("Select", 0);
roiManager("Save", fdir +title+".roi");
A1 = getResult("Area", 0);
A2 = getResult("Area", 1);



Table.create("Result_Cilia");
h = Table.size;
Table.set("Image", h, title);
Table.set("Total Area", h, A1);
Table.set("Thresh Area", h, A2);
Table.set("Ratio", h, A2/A1);


selectWindow(title);
saveAs(fdir +title+ "_kalman05.tif");
//close();
selectWindow("Difference Image");
close();
selectWindow("STD_" + title);
```

7.2. Fluid flow PIV analysis

```
%file location
%path = 'C:\Users\ASUS\Desktop\Resultados\';
path = 'C:\Users\ASUS\Desktop\Resultados\';
%% wt 1
S(1).fname = 'WT_ccdc40_;
S(1).thresh = 0.6;
S(1).ang = 0;


% read file
N = [1];
for pic=1:length(N)
   pic
   coord = ['1C1-' S(N(pic)).fname(1:end-4) '_4.2_TPIV.tsv'];
   leng = ['2C1-' S(N(pic)).fname(1:end-4) '_4.2_TPIV.tsv'];
   ang = ['3C1-' S(N(pic)).fname(1:end-4) '_4.2_TPIV.tsv'];
   img_path = S(N(pic)).fname;

   % read tables
   Tleng = readtable([path leng],'FileType','text');
   Tang = readtable([path ang],'FileType','text');
   Tcoord = readtable([path coord],'FileType','text');
```

```
    img = openimg([path img_path]);

    % process tables
    timep = size(img,3)/3;
    %length
    Tleng1 = Tleng(1:end,3:(timep+1));
    lengdata = table2array(Tleng1);
    square = sqrt(size(Tleng1,1));
    img_size = size(img,1);
    grid = round(img_size/(square+1));


    Tleng1 = reshape(table2array(Tleng1),[square,square,(timep-1)]);
    Tleng1_mean = mean(Tleng1,3);

    %angle
    Tang1 = Tang(1:end,3:(timep+1));
    angledata_deg = rad2deg(table2array(Tang1));
    angledata = table2array(Tang1);
    Tang1_mean = (atan2(mean(sin(angledata),2),mean(cos(angledata),2)));
    Tang1_mean = reshape(Tang1_mean,[square,square]);

    Tang1 = reshape(table2array(Tang1),[square,square,(timep-1)]);

    [x,y] = meshgrid(linspace(grid,img_size-grid,square),linspace(grid,img_size-
grid,square));
    u = Tleng1.*cos(Tang1);
    v = Tleng1.*sin(Tang1);


    %mean

    %circ_mean(angledata(1,:),[],2)
    %circ_mean(angledata(1,:),lengdata(1,:)./max(lengdata(1,:)),2)
    Tang1_mean_weighted = zeros(size(angledata,1),1);
    for i=1:size(Tang1_mean_weighted,1)
        Tang1_mean_weighted(i) =
circ_mean(angledata(i,:),lengdata(i,:)./max(lengdata(i,:)),2);
    end
    Tang1_mean_weighted = reshape(Tang1_mean_weighted,[square,square]);

    u_mean = Tleng1_mean.*cos(Tang1_mean);
    v_mean = Tleng1_mean.*sin(Tang1_mean);


    u_mean_weighted = Tleng1_mean.*cos(Tang1_mean_weighted);
    v_mean_weighted = Tleng1_mean.*sin(Tang1_mean_weighted);


    % quiver
    img_mean = (mean(img(:,:,1:2:size(img,3)),3));
    img_mean_mask = bwareaopen(imfill(
imbinarize(medfilt2(img_mean),S(N(pic)).thresh),'holes'),400);
    %img_mean_mask = imcomplement(img_mean_mask);
    figure('Color','white','Position',[100 100 512 512])
```

```
%imshow(rescale(img(:,:,2)))
box off
%imshow((ind2rgb(rescale(img(:,:,2)),jet)));
%hold on
x_mask = x;
for i=1:size(x,1)
   for j = 1:size(x,1)
      %x(i),y(j)
      if (img_mean_mask(x(i,i),y(j,j)) == 0)
         x_mask(i,j) = NaN;
      end
   end
end
Tleng1_mean_fixed = padarray(Tleng1_mean(3:end-2,3:end-2),[2 2],'replicate');

Tleng1_mean_map = imresize(Tleng1_mean_fixed,[size(img_mean_mask)]);
f= imagesc(Tleng1_mean_map'.*img_mean_mask,[0 6]);
axis square image
f.AlphaData = img_mean_mask;
jet_aux = jet;
jet_aux(1,:) = [0 0 0];
colormap(jet_aux);
box off


%%Give each one its own colormap

%%Then add colorbars and get everything lined up
%q=quiver(x_mask,y,u_mean',-v_mean');
hold on
U = u_mean_weighted';
V = -v_mean_weighted';

U(1,:) = 0;
U(end,:) = 0;
U(:,1) = 0;
U(:,end) = 0;

V(1,:) = 0;
V(end,:) = 0;
V(:,1) = 0;
V(:,end) = 0;

q=quiver(x_mask,y,U,V);
q.Color = 'black';
%quiver(x,y,u(:,:,2)',-v(:,:,2)');


set(gca,'YTickLabel',[]);
set(gca,'XTickLabel',[]);
set(gca,'YTick',[]);
set(gca,'XTick',[]);
hold off

ax = gca;
```

```
    set(ax, 'box','on','XTickLabel',[],'XTick',[],'YTickLabel',[],'YTick',[])
    box on
    ax.XColor = 'black';
    ax.YColor = 'black';
    ax = gca;
    outerpos = ax.OuterPosition;
    ti = ax.TightInset;
    left = outerpos(1) + ti(1);
    bottom = outerpos(2) + ti(2);
    ax_width = outerpos(3) - ti(1) - ti(3);
    ax_height = outerpos(4) - ti(2) - ti(4);
    ax.Position = [left bottom ax_width ax_height];


    exportgraphics(gcf,[S(N(pic)).fname '_plot.png'],'Resolution',300);
    figure,
    div = divergence(x,y,U,V);

    %imagesc(imresize(div,[size(img_mean_mask)]).*img_mean_mask);
    angle_rose = Tang1_mean_weighted';
    angle_rose = angle_rose + deg2rad(S(N(pic)).ang);
    angle_rose = atan2(sin(angle_rose),cos(angle_rose));

    angle_rose(isnan(x_mask))=NaN;
    angle_rose=angle_rose(3:end-2,3:end-2);
    angle_rose(isnan(angle_rose)) = [];
    circ_mean(angle_rose')
    results{pic}.angle = angle_rose;
    polarhistogram(angle_rose,360/30,'normalization', 'probability')


    length_quantif = Tleng1_mean';
    length_quantif(isnan(x_mask))=NaN;
    length_quantif=length_quantif(3:end-2,3:end-2);
    length_quantif(isnan(length_quantif)) = [];
    results{pic}.length = length_quantif;
    %qt(pic) = mean(length_quantif);
end
%% data process

L = results{2}.length';
L =cat(1,L,results{3}.length');
L =cat(1,L,results{11}.length');
L_wt_name = L;
L_wt_name(:) = 1;
L_wt = L;


L = results{4}.length';
L =cat(1,L,results{5}.length');
L =cat(1,L,results{6}.length');
L_bath_name = L;
L_bath_name(:) = 3;
L_bath = L;
```

```
L = results{7}.length';
L =cat(1,L,results{8}.length');
L =cat(1,L,results{9}.length');
L_rescue_name = L;
L_rescue_name(:) = 4;
L_rescue = L;

L = results{10}.length';
L =cat(1,L,results{12}.length');
L =cat(1,L,results{13}.length');
L =cat(1,L,results{14}.length');
L_mut_name = L;
L_mut_name(:) = 2;
L_mut = L;

An = results{2}.angle';
An=cat(1,An,results{3}.angle');
An=cat(1,An,results{11}.angle');
disp('wt')
rad2deg(circ_mean(An))
[wt_N, wt_edg] = histcounts(An,[-pi -2*pi/3 -pi/3 0 pi/3 2*pi/3 pi]);

An = results{4}.angle';
An=cat(1,An,results{5}.angle');
An=cat(1,An,results{6}.angle');
disp('bath')
rad2deg(circ_mean(An))
[bath_N, bath_edg] = histcounts(An,[-pi -2*pi/3 -pi/3 0 pi/3 2*pi/3 pi]);


An = results{7}.angle';
An=cat(1,An,results{8}.angle');
An=cat(1,An,results{9}.angle');
[rescue_N, rescue_edg] = histcounts(An,[-pi -2*pi/3 -pi/3 0 pi/3 2*pi/3 pi]);
disp('rescue')
rad2deg(circ_mean(An))

An = results{10}.angle';
An=cat(1,An,results{12}.angle');
An=cat(1,An,results{13}.angle');
An=cat(1,An,results{14}.angle');
[mut_N, mut_edg] = histcounts(An,[-pi -2*pi/3 -pi/3 0 pi/3 2*pi/3 pi]);
disp('mut')
rad2deg(circ_mean(An))


L_total = cat(1,L_wt,L_bath,L_rescue,L_mut);
%L_total_graph = cat(2,L_wt,L_bath,L_rescue,L_mut);
L_total_name = cat(1,L_wt_name,L_bath_name,L_rescue_name,L_mut_name);
boxplot(L_total,L_total_name)
%%
polar_norm = max([wt_N rescue_N mut_N bath_N]);
figure
polarhistogram('BinEdges',wt_edg,'BinCounts',wt_N/max(wt_N))
rlim([0 1])
```

```
set(gca,'RTick',     [0.2 0.4 0.6 0.8], ...
      'RTickLabel',{0.2 0.4 0.6 0.8})
exportgraphics(gca,['Rose_plot_wt.png'],'Resolution',300);

figure
polarhistogram('BinEdges',bath_edg,'BinCounts',bath_N/max(bath_N))
rlim([0 1])
set(gca,'RTick',     [0.2 0.4 0.6 0.8], ...
      'RTickLabel',{0.2 0.4 0.6 0.8})
exportgraphics(gca,['Rose_plot_bath.png'],'Resolution',300);

figure
polarhistogram('BinEdges',rescue_edg,'BinCounts',rescue_N/max(rescue_N))
rlim([0 1])
set(gca,'RTick',     [0.2 0.4 0.6 0.8], ...
      'RTickLabel',{0.2 0.4 0.6 0.8})
exportgraphics(gca,['Rose_plot_rescue.png'],'Resolution',300);
figure
polarhistogram('BinEdges',mut_edg,'BinCounts',mut_N/max(mut_N))
rlim([0 1])
set(gca,'RTick',     [0.2 0.4 0.6 0.8], ...
      'RTickLabel',{0.2 0.4 0.6 0.8})
exportgraphics(gca,['Rose_plot_mut.png'],'Resolution',300);

%% quiver options


figure
%%Create two axes
ax1 = axes;
[x,y,z] = peaks;
surf(ax1,x,y,z)
view(2)
ax2 = axes;
scatter(ax2,randn(1,120),randn(1,120),50,randn(1,120),'filled')
%%Link them together
hLink =
linkprop([ax1,ax2],{'XLim','YLim','ZLim','CameraUpVector','CameraPosition','CameraT
arget'});
%%Hide the top axes
ax2.Visible = 'off';
ax2.XTick = [];
ax2.YTick = [];
%%Give each one its own colormap
colormap(ax1,'hot')
colormap(ax2,'cool')
%%Then add colorbars and get everything lined up
set([ax1,ax2],'Position',[.17 .11 .685 .815]);
%cb1 = colorbar(ax1,'Position',[.05 .11 .0675 .815]);
%cb2 = colorbar(ax2,'Position',[.88 .11 .0675 .815]);


%%
figure
ax = polarhistogram('BinEdges',[0 pi/3 pi 3*pi/2 2*pi],'BinCounts',[5 3 4 6])
```

```
ax.BinLimits = [0 1];

%%
X = x;
Y = y;

U = u_mean_weighted';
V = -v_mean_weighted';

U(1,:) = 0;
U(end,:) = 0;
U(:,1) = 0;
U(:,end) = 0;

V(1,:) = 0;
V(end,:) = 0;
V(:,1) = 0;
V(:,end) = 0;

U2 = padarray(U,[1 1],0);
figure
imshow(imadjust(img(:,:,1).*uint16(img_mean_mask)));
hold on
q = quiver(X, Y, U, V);

%// Compute the magnitude of the vectors
mags = sqrt(sum(cat(2, q.UData(:), q.VData(:), ...
        reshape(q.WData, numel(q.UData), [])).^2, 2));

%// Get the current colormap
currentColormap = colormap(jet);

%// Now determine the color to make each arrow using a colormap
[~, ~, ind] = histcounts(mags, size(currentColormap, 1));

%// Now map this to a colormap to get RGB
cmap = uint8(ind2rgb(ind(:), currentColormap) * 255);
cmap(:,:,4) = 255;
cmap = permute(repmat(cmap, [1 3 1]), [2 1 3]);

%// We repeat each color 3 times (using 1:3 below) because each arrow has 3
vertices
set(q.Head, ...
   'ColorBinding', 'interpolated', ...
   'ColorData', reshape(cmap(1:3,:,:), [], 4).');   %'

%// We repeat each color 2 times (using 1:2 below) because each tail has 2 vertices
set(q.Tail, ...
   'ColorBinding', 'interpolated', ...
   'ColorData', reshape(cmap(1:2,:,:), [], 4).');
```